The pre-Alpine tectonic history of the Austroalpine continental basement in the Valpelline unit (Western Italian Alps)

PAOLA MANZOTTI*† & MICHELE ZUCALI‡§

*Institut für Geologie, Universität Bern, Baltzerstrasse 1+3, 3012 CH-Bern, Switzerland
‡Dipartimento di Scienze della Terra 'Ardito Desio', Università degli Studi di Milano, Via Mangiagalli, 34 20133
Milano, Italy
§CNR-IDPA – Sezione di Milano, Via Mangiagalli 34 20133, Milano, Italy

Abstract – The Valpelline unit is a large slice of continental crust constituting the Austroalpine Dent Blanche nappe (NW Italy). The pre-Alpine evolution of this unit holds important clues about the Palaeozoic crustal structure at the northern margin of the Adria continent, about the history of rifting in the Alpine region, and thus about the thermomechanical conditions that preceded the Alpine convergent evolution. Several stages of the deformation history and of partial re-equilibration were identified, combining meso- and micro-structural analyses with thermobarometry. Reconstructed pre-Alpine *P*–*T*–*t*–d paths demonstrate that the Valpelline unit experienced an early stage at pressures between 4.5 and 6.5 kbar followed by migmatite formation. A subsequent stage reached amphibolite to granulite facies conditions. This stage was associated with the development of the most penetrative fabrics affecting all of the Valpelline lithotypes. The pre-Alpine evolution ended with a weak deformation associated with a local mineral-chemical re-equilibration under greenschist facies conditions at $\approx$ 4 kbar and $T < 450\,°C$. A Permo-Mesozoic lithospheric extension is thought to be responsible for asthenosphere upwelling, thereby causing high temperature metamorphism at medium pressure and widespread partial melting, which led to upper crustal magmatic activity.

Keywords: Valpelline unit, pre-Alpine metamorphism, Austroalpine, Permian, geodynamic evolution.

1. Introduction

Granulite-facies rocks contain a unique record of lithosphere-scale structural and metamorphic history, and granulite terranes reflect major tectonic processes in the deep Earth (Green & Ringwood, 1967; Bohlen, 1987; Ellis, 1987; Harley, 2008). Granulite-facies rocks and migmatite production are associated with extensional regimes (Pin & Vielzeuf, 1983; Lardeaux & Spalla, 1991; Marschall, Kalt & Hanel, 2003; Schuster & Stüwe, 2008) as well as with compressional regimes, where they are likely related to crustal shortening, high isotopic heat production and coeval erosional unroofing (Gruf Complex, Central Alps: Galli *et al.* 2012; e.g. Himalaya: Searle *et al.* 2010).

A Carboniferous amphibolite to granulite facies evolution is well established in the Variscan belt (Pin & Vielzeuf, 1983, 1988; Marschall, Kalt & Hanel, 2003). Slices of these Variscan belt granulites have been incorporated in the Alpine chain within the external or axial units (von Raumer, Stampfli & Bussy, 2003; Marotta & Spalla, 2007; Schuster & Stüwe, 2008). Within the internal units of the Alpine chain, Permian–Triassic magmatism and amphibolite–granulite metamorphism have also been described (Marotta & Spalla, 2007). There are two main groups of interpretations of this post-Carboniferous thermal anomaly: (i) as an effect of the late orogenic collapse

of the Variscan belt (Malavielle *et al.* 1990; Ledru *et al.* 2001) and (ii) as a consequence of lithospheric thinning and asthenosphere upwelling that led to continental rifting (Lardeaux & Spalla, 1991; Diella, Spalla & Tunesi, 1992; Müntener & Hermann, 2001; Schuster & Stüwe, 2008; Marotta, Spalla & Gosso, 2009).

The aim of the present study is to reconstruct the pre-Alpine tectonometamorphic evolution of the Valpelline unit (Dent Blanche nappe, Western Italian Austroalpine Domain) pre-dating the beginning of the Alpine convergence. The Valpelline unit represents one of these Variscan slices incorporated into the Alpine chain. Rocks from a small side canyon of Valpelline Valley have been selected for this purpose because the pre-Alpine structures and assemblages are well preserved as a result of the poor Alpine deformation affecting this part of the Valpelline unit. Pressure–temperature–time–deformation (*P*–*T*–*t*–d) paths have been derived by combining the sequence of deformational stages with the successive metamorphic imprints. Our results suggest a tectonometamorphic evolution of the Valpelline unit that differs from that described in previous studies.

2. Geological setting

The Alps are a double vergent orogen. They formed since the Cretaceous period as a consequence of the convergence between Europe and the Adria-Africa plates and the closure of an oceanic basin, the Tethys,
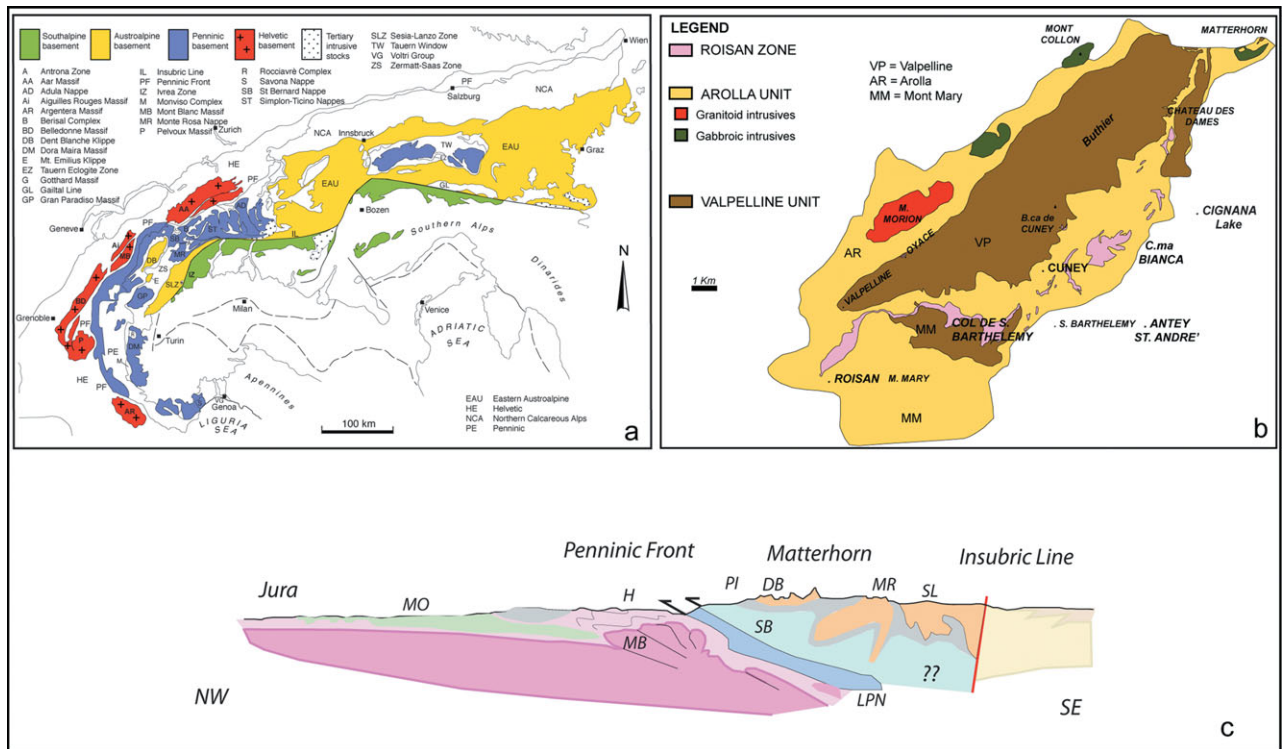
†Author for correspondence: manzotti@geo.unibe.ch

Figure 1. (Colour online) (a) Tectonic map of the Alps (modified after Marotta & Spalla, 2007). (b) Simplified geological map of the Dent Blanche tectonic system (Roda & Zucali, 2011). (c) NW–SE geological cross-section along the Western Alps: SL – Sesia-Lanzo Zone; MR – Monte Rosa; DB – Dent Blanche; PI – Penninic; SB – Grand Saint Bernard; MB – Mont Blanc; LPN – Lower Penninic; H – Helvetic; MO – Molasse (Zucali, 2011).

that was interposed between the two continental passive margins (Malusà *et al.* 2011). The axial part of the Alps is formed by fragments of continental- and ocean-derived rocks, which suffered, from the Cretaceous to Oligocene periods, important vertical and horizontal movements and associated high pressure–low temperature (HP–LT) metamorphism owing to subduction and collision processes (Fig. 1). The continental basement units derived from the Adriatic margin are referred to Austroalpine units. The Dent Blanche nappe (Western Italian Alps) belongs to this domain (Fig. 1). This nappe is composed of pre-Alpine continental crust belonging to the African plate that heterogeneously recorded two tectonic and metamorphic stages of evolution: the pre-Alpine and the Alpine imprint (Caby, Kienast & Saliot, 1978; Ballèvre & Kienast, 1987; Canepa *et al.* 1990; De Giusti, Dal Piaz & Massironi, 2003). The former is characterized by superimposed deformation stages associated with high temperature and high to intermediate pressure metamorphic imprints (granulite facies and amphibolite–granulite facies). The Alpine cycle is related to a low temperature and intermediate pressure metamorphic imprint (blueschist–greenschist facies) associated with superimposed mylonitic foliations (Roda & Zucali, 2008). As classically defined, the Dent Blanche nappe comprises a Palaeozoic basement and lenses of Mesozoic metasedimentary cover (i.e. the Roisan Zone and the Mt Dolin unit). The basement includes the Arolla Series and the Valpelline Series (Argand, 1906; Diehl, Masson & Stutz, 1952) from since-named units (Manzotti, 2011).

The Arolla unit is mainly composed of Permian-age granite, clinopyroxene-bearing granite, diorite, gabbro metamorphosed and deformed during the Alpine tectonometamorphic evolution to orthogneiss, chlorite-white mica-amphibole-bearing gneiss and schist (De Leo, Biino & Compagnoni, 1987; Pennacchioni & Guermani, 1993; Roda & Zucali, 2008). Within unde-formed igneous cores, 1 m to 10 m sized xenoliths of biotite-sillimanite-bearing gneisses and amphibolites occur as remnants of pre-Alpine high temperature evolution (Diehl, Masson & Stutz, 1952; Pennacchioni & Guermani, 1993; Roda & Zucali, 2008). The Arolla unit primarily records the Alpine tectonometamorphic evolution, whereas the pre-Alpine imprint is restricted to 1 to 10 m scale relics. Radiometric determinations on zircons of the Arolla unit orthogneiss indicate an age of 289 ± 2 Ma for their igneous protoliths (Bussy *et al.* 1998).

The Valpelline unit comprises pre-Alpine high-grade (amphibolite- to granulite-facies) paragneisses with lenses and layers of basic granulites, garnet-clinopyroxene-bearing amphibolites and marbles (Diehl, Masson & Stutz, 1952; Gardien, Reusser & Marquer, 1994).

The dominant metamorphic imprint occurs under amphibolite to granulite facies conditions, and it is of pre-Alpine age (Gardien, Reusser & Marquer, 1994). The Alpine imprint is weak and localized along high-strain zones that are tens to hundreds of metres wide. A static greenschist facies re-equilibration related to the development of an Alpine foliation is observed

in certain places (Diehl, Masson & Stutz, 1952; Kienast & Nicot, 1971; De Leo, Biino & Compagnoni, 1987; Roda & Zucali, 2008). Kienast & Nicot (1971) also described kyanite-chloritoid Alpine assemblages. Hunziker (1974) obtained ages of between 200 and 180 Ma for the Valpelline unit using the K–Ar and Rb–Sr methods on biotites. An age of 135 Ma has been derived using the K–Ar method on muscovites, and this age most likely related to a successive Alpine re-equilibration (Hunziker, 1974; Gardien, Reusser & Marquer, 1994; Roda & Zucali, 2008) or may also be interpreted as a mixed age resulting from an incomplete re-equilibration between pre-Alpine and Alpine white micas.

The northeastern part of the Valpelline Valley is characterized by high-grade paragneisses with interlayered basic granulites, Grt-Cpx-bearing amphibolites and marbles (Diehl, Masson & Stutz, 1952; Gardien, Reusser & Marquer, 1994). Anatectic veins and dykes of garnet-bearing pegmatite are common (Diehl, Masson & Stutz, 1952; Pennacchioni & Guermani, 1993). Low- to medium-grade micaschists with interlayered calc-silicate bands occur in the southwestern part (Pennacchioni & Guermani, 1993). Metapelites are generally banded, and foliation is defined by the alternation of dark (biotite and garnet) and light (quartz and plagioclase) layers and by the shape preferred orientation (SPO) of biotite and sillimanite (Gardien, Reusser & Marquer, 1994). Generally, the mineral assemblage of these gneisses consists of garnet, sillimanite, biotite, plagioclase, quartz, rutile, oxide, feldspar, muscovite and cordierite (Diehl, Masson & Stutz, 1952; Gardien, Reusser & Marquer, 1994). The lithological boundaries are generally parallel to the dominant foliation, which is marked by biotite and sillimanite in gneiss, amphiboles and plagioclase in amphibolite, and calcite and clinopyroxene in marble. This penetrative foliation can be traced for several kilometres along the valley, making this structure a robust chronological benchmark. This foliation is locally bent: folds that range from metres to decametres in size are tight to isoclinal, and they are often associated with the development of a new axial plane foliation.

Thermobarometrical estimates for the Valpelline unit indicate a first stage at $T = 700–800\,°C$ and $P = 9–10$ kbar characterized by the growth of kyanite prior to the migmatite stage at $T = 800–850\,°C$ and $P = 6–7$ kbar, which follows an amphibolite re-equilibration stage at $T = 750–800\,°C$ and $P = 5–6$ kbar (Gardien, Reusser & Marquer, 1994). The high temperature pre-Alpine evolution ends with a static stage of re-equilibration at $T = 650–750\,°C$ and $P = 3–5$ kbar (Gardien, Reusser & Marquer, 1994; Gardien, 1994). Greenschist facies conditions ($T = 450–500\,°C$, $P = 3–4$ kbar) are recorded in all lithologies but cannot be easily attributed to the pre-Alpine or Alpine cycles (Roda & Zucali, 2008; Manzotti, 2011). The similar pressure and temperature conditions recorded by the two units suggest that they underwent a comparable polycyclic evolution. At present, the contact between the Valpelline and Arolla units is notably sharp: the transition occurs in a few tens of metres, and it is marked by Alpine-age greenschist-facies mylonites and cataclasites (Pennacchioni & Guermani, 1993).

We focused our study on rocks cropping out in a small canyon (Fig. 2; UTM WGS84 coordinates: 372874–5077575; 373168–5077213), which is 8–10 m wide and approximately 400 m long (between 1080 m and 1300 m altitude). This canyon is situated on the northern flank of Valpelline Valley between the villages of Valpelline and Oyace, close to Thoules. In this area, the older stages of the structural evolution, pre-dating the dominant foliation, are preserved in metre-scale basic granulite boudins wrapped in migmatites.

3. Approach and methods used

Because the geological history of a metamorphic terrane is generally composed of successive or contemporaneous magmatic, metamorphic and deformational evolutionary stages (hereafter simply referred to as stages), we approached the reconstruction of metamorphic terranes by separating each stage on the basis of its characteristics at meso- and microscopic scales following the approach described by Spalla *et al*. (2005, 2010). The relative timing of structures inferred by superimposed fabric elements (Turner & Weiss, 1963) and the analysis of the mineral assemblages marking each fabric element allow for the definition of the relative timing of structures within each lithology (i.e. phases of deformation, such as D_1 and D_2) with respect to the metamorphic conditions in which they developed.

Criteria for structural correlation among all stages were applied at 1:100 to 1:400 mapping scales (Turner & Weiss, 1963; Passchier & Trouw, 2005). Data are represented in a structural-metamorphic map in which lithotypes and fabric elements are highlighted (Fig. 8).

Microstructural analysis was used to identify the metamorphic assemblages, to study the correlation between deformation and metamorphism, and to select areas of special interest to be used for chemical microprobe analyses and $P–T$ calculations. Mineral phases have also been chronologically distinguished (e.g. GrtI, GrtII) using as indicators their microstructural positions, optical characters and relative growth microstructures (Vernon, 2004; Passchier & Trouw, 2005; Vernon & Clarke, 2008). In some cases, the relative chronology of the single mineral phases does not correspond to the stage chronology (e.g. GrtII in stage 3), and in large part, this chronology has been validated by the chemical compositions of the mineral phases and by thermobarometrical estimates. Large- and small-scale processes may be linked by combining these different techniques and exploiting the heterogeneous distribution of metamorphism and deformation. The relative chronology of $P–T$ estimates is subsequently used to reconstruct the $P–T–t$–d paths, and the tectonometamorphic evolution of the Valpelline
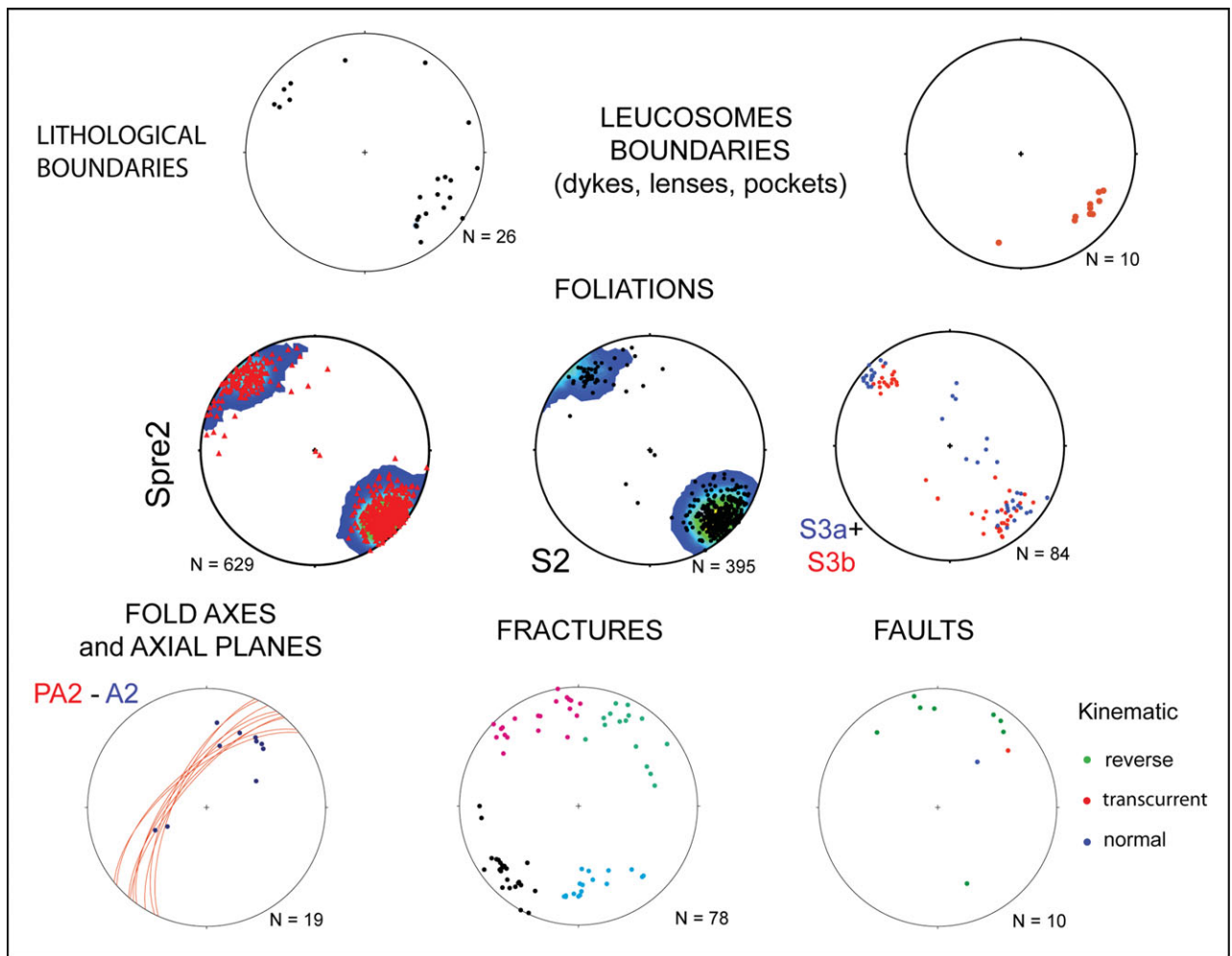
Figure 2. (Colour online) Lower hemisphere Schmidt (equal area) projections of the structures recognized in the studied area.

unit rocks will be presented thereafter in the pre-Alpine tectonic and geodynamic framework.

Mineral abbreviations are in accordance with Whitney & Evans (2010); in addition, white mica is abbreviated as Wm, and opaque minerals abbreviated as Op.

4. Meso- and microstructures and their mineral support

4.a. Rock types and their relationships

The area is dominated by metapelites (migmatite and Bt-bearing gneiss), metabasites (basic granulite and amphibolite), Ol-bearing marbles and Grt-bearing leucosomes (Fig. 3).

Migmatites (Fig. 3a) consist of metatexites in which leucosomes may occur as centimetre-sized spots; granoblastic aggregates of Qz + Kfs + Pl + Grt ± Crd (Fig. 3b) are commonly oriented parallel to the dominant foliations. Locally, the leucosomes may be more prominent and continuous, defining centimetre- to metre-thick layers associated with variably thick melanosomes. Melanosomes are generally flat, and the major constituents are Bt, Grt and Sil. Locally, Grt-rich restites occur with a modal amount of > 50–60 %. Bt-bearing gneisses are characterized by fine to medium grains and display a pervasive foliation. Millimetre- to centimetre-thick Qz-Fsp lithons are alternated with millimetre-thick Bt films. Locally, Grt-rich layers are also present and are parallel with Bt films and Qz-Fsp lithons.

Opx-bearing basic granulite and amphibolite occur as metre-scale boudins within migmatite (Fig. 3a, b) or as decametre-scale bodies interlayered with pelitic migmatites and Bt-bearing gneisses. Opx-granulites are characterized by fine to medium grains and show granoblastic texture. These rocks are commonly massive, and a weak foliation marked by the Pl- and Grt-rich layers is only locally observed at the boundaries of the granulite boudins (Fig. 3a).

Grt-bearing leucosomes (i.e. pegmatites, according to Diehl, Masson & Stutz, 1952) occur at the boundaries between migmatites and basic boudins (Fig. 3a, c, d).

The mineralogical compositions and the amounts of each mineral in different lithologies are reported in Table 1.

4.b. Stages of evolution

In the studied area, four evolutionary stages have been recognized at the meso- and micro-scale. The
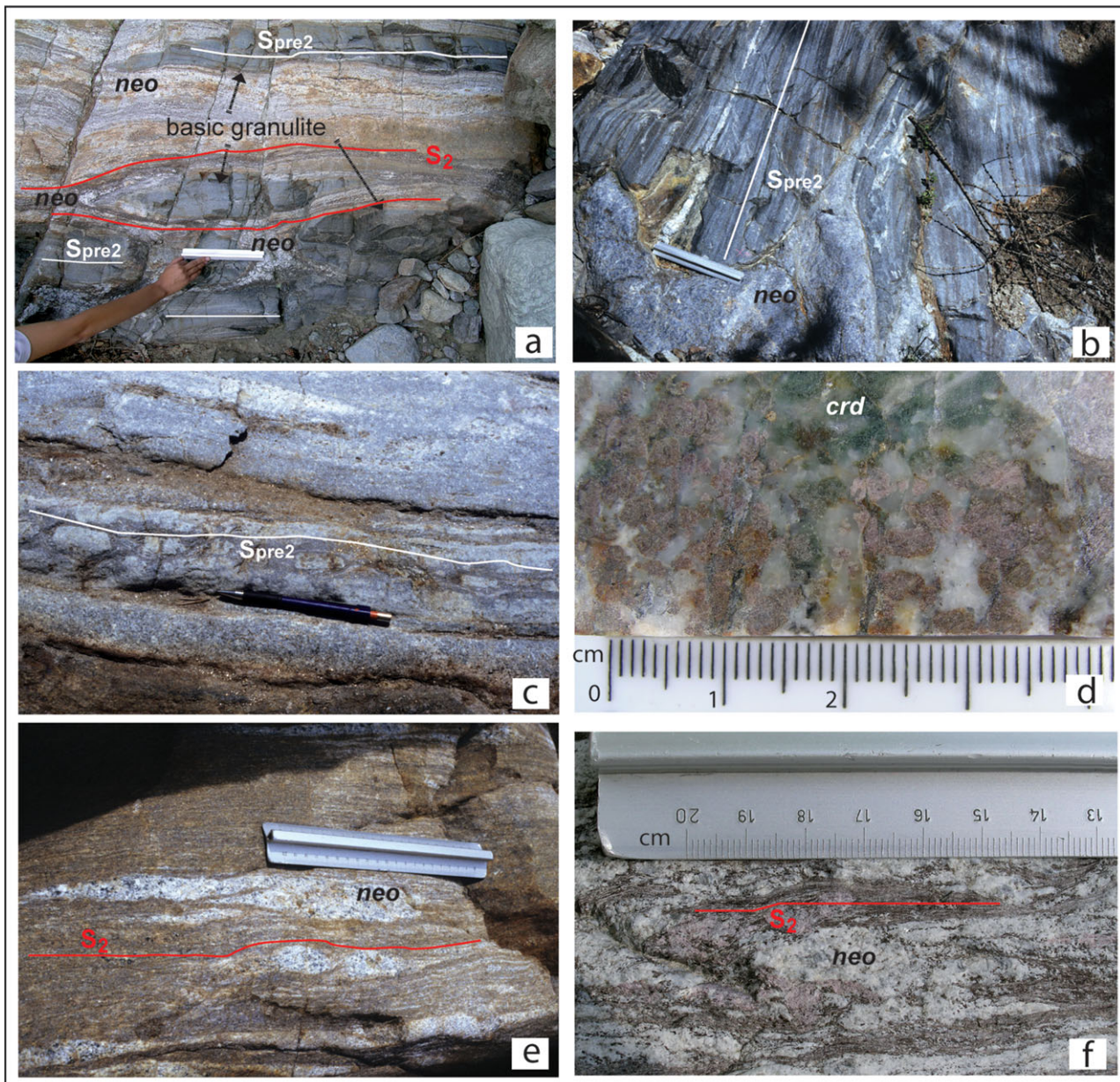
Figure 3. (Colour online) Field photographs of metapelites and metabasites of the Valpelline unit. (a) Opx-bearing basic granulite lens in migmatites. In migmatites proximal to the contact with basic granulite a centimetre-thick Fsp-Grt-rich neosome (neo) occurs. (b) Amphibolite: S_{pre2} is marked by centimetre-thick layers, respectively, of Pl, black-brown Amp and white-green Amp. A leucosome pocket, associated with stage 2, cuts this structure. (c) Ol-bearing marble layer with a weak S_{pre2} foliation. (d) Granoblastic aggregate of Qz + Grt + Pl + Crd in a leucosome. (e, f) Migmatites: stage 2 melanosomes and leucosomes alternate. Leucosomes, produced by stage 2, contain Qz, Fsp and locally Grt.

unravelled structural and metamorphic evolution is summarized in the following paragraphs, whereas Table 2 synthesises the superimposed mesostructures and their relative relationships. The orientations of fabric elements are plotted on Schmidt diagrams in Figure 2.

In Figures 4 and 5, the relationships between microstructural evolution and metamorphic growth are summarized. Table 3 reports stable metamorphic assemblages, which are chronologically ordered on the basis of the following microstructural analysis. The subscript associated with each mineral group refers to the relative timing of growth and not to the stages. The map in Figure 8 displays lithological associations and

superimposed foliations together with indications of the fabric-supporting minerals.

4.b.1. Stage pre2

Stage pre2 is characterized by structures that are clearly prior to stage 2. This stage is locally recognizable in different lithologies (e.g. boudins of Opx-bearing granulites wrapped within pelitic migmatites (Fig. 3a), amphibolite (Fig. 3b) and Ol-bearing marbles (Fig. 3c)). Stage pre2 likely comprises various events, as locally testified by the different metamorphic assemblages associated with the structures (e.g. amphibole marking a S_{pre2} foliation in amphibolite and orthopyroxene

Table 1. Mineralogical compositions and amount of each mineral in the different lithologies

Rock Type	Minerals and %	
Pelitic migmatite	Grt (20), Wm (15), Sil (10–15), Pl (10), Crd (10), Qz (10), Chl (10), Ep (5–10), Bt (5–10), Rt (5), Ap (5), Cal (< 5), Zrn (< 5), Mnz (< 5)	metapelite
Bt-bearing gneiss	Fsp (30–35), Qz (30), Bt (15–20), Grt (10–15), Rt (< 5), Zrn (< 5), Mnz (< 5)	
Zrnx-bearing basic granulite	Cpx (15), Zrnx (15), Pl (20), Am (10), Bt (5–10), Zrn (5), Wm (5), Chl (< 5), Tur (< 5)	metabasite
Amphibolite	Brown Am (25–30), Pl (15–20), Grt (15), Wm (15) white-green Am (10–20), Chl (5–10), Ep (5–10), Zrn (5), Qz (<5), Ap (< 5)	
Ol-bearing marble	Cal (40–50), Qz (5–10), Wm (5–10), Ol (5–10), Srp (0–5), Grt (0–5), Px (0–5), Chl (0–5), Ep (0–5)	marble
Grt-bearing leucosome	Pl (20), Kfs (20), Qz (15), Wm (15), Bt (10), Grt (5–10), Chl (5–10), Ep (5), Zrn (< 5), Mnz (< 5)	leucosome

Table 2. Schematic relationships between deformation and metamorphism in the Valpelline Unit

Relative chronology of mesostructures and their mineral support

Stage	Events	Age	Structures	Mineral associations
pre2	Met-pre2+D-pre2	Pre-Alpine	Inequigranular aggregates; S_{pre2}	Opx-Cpx-Pl (basic granulite); amphibolite, Ol-bearing marble
2	Met2+Mag2+D2	Pre-Alpine	Metric migmatite structures (S_2); reaction rims at basic boudin boundaries	Sil-Bt-Grt melanosome and Qz-Pl-Kfs-Grt-Bt±Crd leucosome Opx-Cpx-Pl ± Amp ± Grt (basic granulite) Qz-Pl-Kfs-Grt-Bt leucosome
3	Met3a+D3a Met3b+D3b	Pre-Alpine	Folds and foliations (S_{3a}) Folds and foliations (S_{3b}; F_{3b}; AP_{3b} L_{3b})	Bt-Kfs-Qz-Sil-Grt; Am-Pl Bt-Kfs-Qz-Sil-Grt Am-Pl Cc-Ol-Phl-Cpx
4	Mag3 Met4 + D4	Alpine	Intrusive boundaries Coronas Fracture, faults and veins	Leucosome or lenticular intrusions Static growth of Chl, Wm, Ep Chl-Ep-rich veins

Met – metamorphic; D – deformational; Mag – magmatic.
S – foliation; L – lineation; F – fold; AP – axial plane.

layers developing in basic granulite). For this reason, we only refer to stage pre2 in reference to all structures pre-dating stage 2. Parts a–c and e of Figure 3 show the geometric overprinting relationships between stage 2 structures (e.g. S_2 foliation, boudinage and melt pocket) and those pre-dating them.

4.b.1.a. Meso-scale observations

D_{pre2} structures are more evident in Opx-bearing granulite boudins, amphibolites and marbles and mainly consist of a weak centimetre- to millimetre-thick S_{pre2} foliation. S_{pre2} in granulites are rare; where present, they are marked by a gentle SPO of Pl, Cpx and Opx.

In amphibolites, the S_{pre2} foliation is defined by centimetre-thick mineralogical layers alternating between Amp- and Pl-rich. The SPO of Amp also defines this structure (Fig. 3b).

4.b.1.b. Micro-scale observations

In basic granulites, an inequigranular polygonal to interlobate texture is preserved. It is characterized by subhedral crystals of OpI, BtI and ApI and by clustered polygonal to interlobate aggregates of PlI, CpxI and

OpxI (Fig. 4a). Euhedral to subhedral OpxI and CpxI are commonly prismatic in shape, ranging from millimetres to centimetres in size with well-defined and straight grain boundaries. BtI occurs as single grains (0.5–1 mm) and locally shows undulose extinction. OpI and ApI occur as millimetre-sized single crystals in close association with OpxI, CpxI and PlI.

In Bt-gneisses, stage pre2 is also preserved; it occurs within metre-sized volumes where aggregates of QzI + PlI + KfsI + BtI + GrtI ± SilI are recognizable. QzI occurs as strained grains or aggregates with undulose extinction and deformation bends. PlI shows a prismatic anhedral to subhedral habit up to several millimetres in size, and it is characterized by deformational features such as undulose extinction and deformation twinning. QzI and PlI form microlithon domains that are elongated to BtI aggregates. BtI and rarely SilI form microfilm domains. GrtI crystals are wrapped by the main foliation marked by the SPO of BtI ± SilI and by QzI elongate aggregates. GrtI occurs as millimetre-sized euhedral grains with inclusions of Qz and BtI (Fig. 4b). ZrnI is commonly found as euhedral prismatic crystals with high relief and
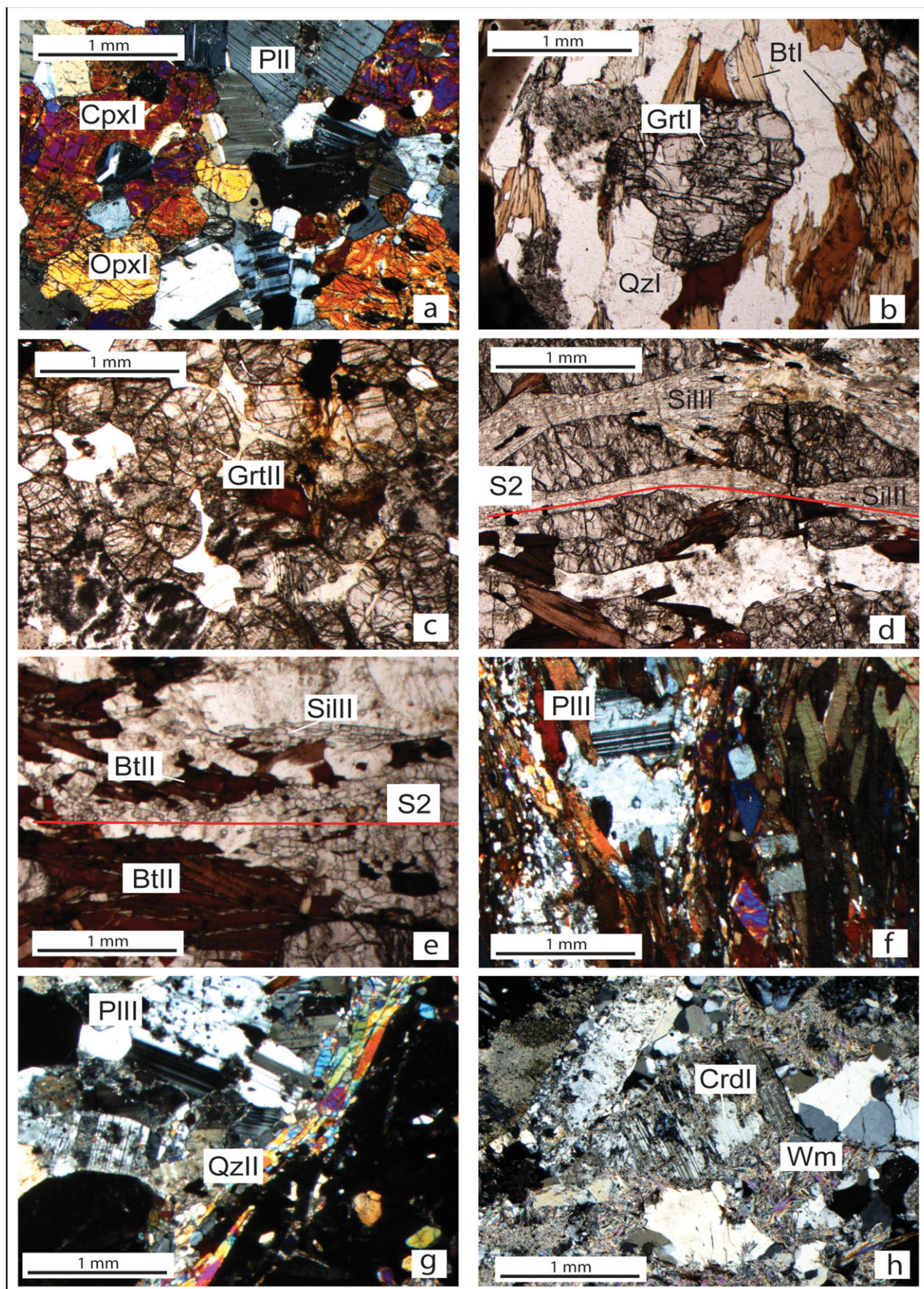
Figure 4. (Colour online) Photomicrographs of observed microstructures of metapelites and metabasites of the Valpelline unit. (a) Basic granulite: polygonal to interlobate aggregate of CpxI, OpxI and PlI (crossed polars). (b) Bt-bearing gneiss: GrtI occurs as an inclusion-rich core within the S_{pre2} foliation (plane-polarized light). (c) Pelitic migmatite: millimetre-sized rounded grains of GrtII in a melanosome (plane-polarized light). (d) Pelitic migmatite: aggregates of large fibrolitic SilII partly truncate GrtII rims and define the
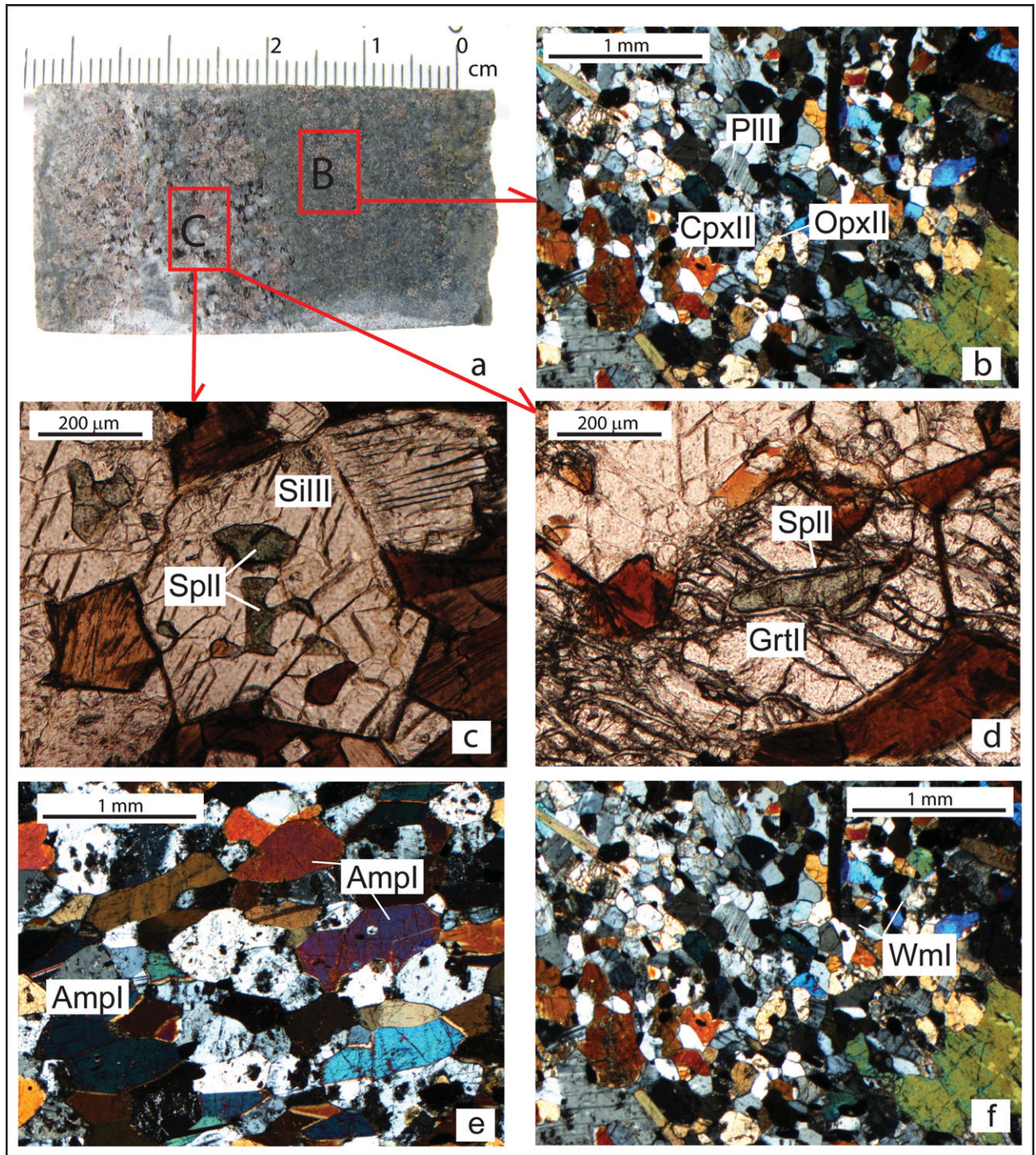
Figure 5. (Colour online) (a) Contact (C) between pelitic migmatite and a lens of basic granulite (B). (b) Basic granulite at the contact with migmatite: interlobate aggregate of OpxII + CpxII + PlII (crossed polars). (c, d) Pelitic migmatite at the contact with basic granulite: SpI + GrtII and SpI + SilII aggregates (plane-polarized light). (e) Amphibolite: shape preferred orientation of AmpI defines the S_{3a} foliation (crossed polars). (f) Pelitic migmatite: Grt porphyroblasts with WmI-filled fractures (crossed polars).

birefringence, and they are frequently associated with GrtI. MnzI occurs as rounded, high-relief crystals with high birefringence associated with SilI or as inclusions in GrtI and BtI.

Therefore, the association of BtI + QzI + PlI + KfsI + GrtI + ZrnI + MnzI + RtI + ApI ± SilI defines the relict S_{pre2} foliation in metapelites (Table 3).

S_2 foliation (plane-polarized light). (e) Pelitic migmatite: SilII aggregates partly replace BtII (plane-polarized light). (f) Pelitic migmatite: subhedral crystal of PlII with growth twins (crossed polars). (g) Pelitic migmatite: leucosome with a coarse-grained granoblastic texture, characterized by PlII, KfsII and QzII (crossed polars). (h) Pelitic migmatite: CrdI crystals are replaced by aggregates of Wm (crossed polars).

Table 3. Pre-Alpine and Alpine deformational, magmatic and metamorphic events (D, Mag, Met) of the Valpelline rocks, recognized at the microscale. Metamorphic assemblages marking each fabric are also described

Microstructures and metamorphic assemblages

Stage	Microstructures	Fabric Supporting Minerals	Rock Type
pre2	granoblastic texture	OpxI + CpxI + PlI + OpI + BtI + ApI	basic granulite
	relict Spre2 foliation	BtI + QzI + PlI + KfsI + GrtI + ZrnI + MnzI + RtI + ApI ± SilI	gneiss
2	S2	LEUCOSOME: QzII + PlII + KfsII + GrtII ± CrdI + BtII + MnzII + ZrnII	migmatite
		MELANOSOME: GrtII + SilII + QzII + PlII + KfsII + BtII + MnzII + ZrnII + RtII	migmatite
		OpxII + CpxII + PlII + GrtII	migmatite–granulite boundary in granulite
		Melanosome association + Spl - GrtII or Spl - SilII	migmatite–granulite boundary in migmatite
		AmpI + PlII + GrtII + CpxII + QzI+ OpI	basic granulite
3	D3a + S3a - D3b + S3b	BtII + SilII + QzII + KfsII + PlII + GrtII + RtIII + ZrnII + MnzII	migmatite
		AmpI + PlII + GrtII + CpxII + QzI+ OpI	basic granulite/amphibolite
	equigranular aggregates – igneous textures	KfsIII + QzIII + BtIII + GrtIII + RtIII + MnzIII + ZrnIII	pegmatite
4	reaction rims – pseudomorph aggregates – fractures	WmI - AmpII - ChlI - EpI - CalI	all

4.b.2. Stage 2

During stage 2, migmatite fabrics develop in metapelites. Contemporaneously, basic granulites and amphibolites partly or completely change their mineral associations; such reactions are localized at the basic boudin boundaries where stage 2 neosomes localize (Fig. 3a; Table 2). This stage is not recorded in marbles, whereas it is maximally developed in metapelites.

4.b.2.a. Meso-scale observations

In pelitic migmatite, D_2 structures consist of centimetre- to millimetre-thick S_2 foliation, expressed by alternating layers of leucosomes (Fig. 3d) and melanosomes (Figs 3e, f). The leucosomes are disharmonically folded and boudined in the fold limbs. The leucosomes hold their granoblastic structure, even where folded during D_2. The melanosomes are variable in width and are composed of Sil, Grt, Bt, Pl and Kfs. The SPOs of Sil and flattened Grt layers define the S_2 foliation in melanosomes together with the SPO of Bt (Fig. 3f). Marble, amphibolite and granulite boudins are wrapped by the S_2 foliation at decimetre to metre scales. Centimetre-thick leucosomes are also localized along the boundaries between granulite-amphibolite boudins and migmatites (Figs 3a, b). These boundaries are usually parallel to the S_2 foliation that it is marked by Bt + Sil-rich layers in migmatites and by the increase in the amount of Grt and Amp within granulite and amphibolite boudins. In amphibolite boudins, S_{pre2} foliation generally tends to be folded and parallel to the external S_2 foliation, especially at their margins, as is also shown by stereographic projection in Figure 2.

4.b.2.b. Micro-scale observations

In pelitic migmatite, melanosomes and leucosomes are easily distinguished by their textures: leucosomes are defined by granoblastic polygonal aggregates of QzII + PlII + KfsII + GrtII + BtII, whereas melanosomes preserve a spaced foliation marked by the SPO of BtII + QzII + GrtI/II + SilII. At the micro-scale, the distinctive character of the melanosomes is the high modal proportion of residual and accessory minerals, such as Grt and Sil. GrtII occurs as millimetre- to centimetre-sized grains, locally zoned (Fig. 4c); the inner part (i.e. GrtI) is rich in inclusions of RtI, QzI, BtI and SilI, whereas the outer part (GrtII) is inclusion-free. Large and rounded inclusions of QzI and BtI are common in GrtI, as are aggregates of BtI + SilI; such relationships may be interpreted as the relics of the older reactant assemblage (Sawyer, 2008; Kriegsman & Alvarez-Valero, 2010). The rims of GrtII may be partly truncated or dissolved by aggregates of large, fibrolitic SilII (Fig. 4d). S_2 foliation, marked by the SPO of SilII, BtII and minor QzII, KfsII and PlII, is generally well developed in melanosomes. BtII has a more homogeneous appearance than BtI: it is more reddish in colour and commonly is not internally strained. BtII may be partly replaced by SilII (Fig. 4e). SilII occurs as prismatic porphyroblasts or as elongate fibrolitic domains defining S_2 foliation (Fig. 4e). Euhedral crystals of SilII may occur in association with GrtII rims and BtII and indicate a likely reaction involving SilII as a product of GrtII and BtII. This reaction is also suggested by the presence of SilII aggregates, generally parallel to S_2 foliation, at the rims of GrtII; these microstructural relationships are commonly found in melanosomes close to leucosomes containing microstructures that indicate crystallization from melt (see below). PlII (0.5–6 mm) forms subhedral or anhedral crystals, and many of them show growth twins (Fig. 4f), suggesting growth from melt (Vernon, 2004; Sawyer, 2008), whereas few grains are characterized by undulose extinction, deformation bands and twins. RtII may occur as millimetre-sized single crystals or as inclusions within BtI and BtII. ZrnII and MnzII are also enclosed within QzII and SilII.

Leucosomes display coarse-grained granoblastic textures; PlII, KfsII and QzII constitute the main frame of the texture (Fig. 4g). The interstitial space

is filled by QzII, KfsII and BtII, thereby defining thin films. GrtII and BtII crystals that occur in the leucosome are relatively strain-free euhedral grains. Locally, millimetre-sized CrdI porphyroblasts occur, but they have generally been replaced by aggregates of Wm (Fig. 4h). MnzII and ZrnII occur in association with QzII, BtII and GrtII.

Consequently, the assemblages marking the fabrics developed during stage 2 and thus interpreted as stable during this stage are as follows (Table 3):

Melanosomes: *GrtII + SilII + QzII + PlII + KfsII*
  + BtII + MnzII + ZrnII + RtII
Leucosomes: *QzII + PlII + KfsII + GrtII ± CrdI*
  + BtII + MnzII + ZrnII

Marble, amphibolite and granulite boudins are wrapped by the S_2 foliation at decimetre to metre scales. Centimetre-thick leucosomes are also localized along the boundaries between granulite-amphibolite boudins and migmatites (Fig. 3a, b). These boundaries are usually parallel to the S_2 foliation that it is marked by Bt+Sil-rich layers in migmatites and by the increase in the amount of Grt and Amp within granulite and amphibolite boudins. In amphibolite boudins, S_{pre2} foliation generally tends to be folded and parallel to the external S_2 foliation, especially at their margins (Fig. 3e), as is also shown by stereographic projection in Figure 2.

Stage 2 is also recorded at the contact between migmatites and lenses of basic granulites (Fig. 5a). The recrystallization of Opx, Cpx and Pl occurs in basic granulite, developing OpxII + CpxII + PlII + GrtI polygonal or interlobate inequigranular aggregates (Fig. 5b). In the central portions of basic granulite, S_2 is expressed by the SPO of Amp and by Pl layers. In the corresponding migmatite, S_2 is a spaced foliation marked by GrtII-rich bands alternating with PlII–QzII-rich layers. The SPO of BtII also marks this structure. PlII crystals (2–6 mm) show growth and deformation twins, and the grain boundaries are straight and rational. BtII grains are generally euhedral and define Bt-rich layers that commonly rim GrtII bands and PlII–QzII layers. Spl + GrtII and Spl + SilII aggregates may locally occur (Fig. 5c, d). Spl is found as anhedral crystals (0.5–2 mm) with amoeboid grain boundaries.

4.b.3. Stage 3

Stage 3 is characterized by two superimposed deformational phases that rework the pre-existing structures. Both deformational phases are marked by the same metamorphic minerals, thereby supporting the decision to group them into a single stage.

4.b.3.a. Meso-scale observations

During stage D_{3a}, the S_2 foliation is folded, and a new axial plane foliation S_{3a} develops. In migmatites, S_{3a} is marked by the SPO of Bt and Sil aggregates,

which are associated with Grt grains and are frequently elongated parallel to this structure. In granulites, S_{3a} is marked by dark, centimetre-thick Amp ± Bt layers and light, millimetre- to centimetre-thick Pl–Cpx layers. In amphibolites, S_{3a} is expressed by alternating millimetre- to centimetre-thick Pl- and Amp-rich layers. In certain cases, S_{3a} is also marked by the SPO of Amp and by layers and lenses constituted by Grt and green-grey Cpx. In marbles, the SPO of carbonate and locally Qz- and Cpx-rich layers usually define this fabric. The orientation of the S_{3a} foliation is generally settled in an area of 25–30 km^2 and is roughly parallel to the lithological boundaries (see the stereographic projections in Fig. 2).

Stage D_{3b} is associated with close to isoclinal folds in all lithotypes. In migmatites and amphibolites, the D_{3b} deformation phase may be locally associated with the development of a new axial plane foliation, S_{3b}, which is visible at the decametre to metre scale. Generally, S_{3a} and S_{3b} are marked by the same minerals, and they may be easily recognized only where superimposed relationships are preserved. Associated with this phase of deformation, centimetre- to metre-thick Bt + Grt-bearing leucosomes occur, cross-cutting lithological boundaries and S_2, S_{3a} and S_{3b} foliations or locally parallel to S_{3a} or S_{3b} structures. Such geometrical relationships suggest a development during the final stage of D_3.

4.b.3.b. Micro-scale observations

D_{3a} structures are well recorded in migmatites. S_{3a} is a spaced foliation marked by BtII + GrtII layers and by QzII + PlII + KfsII lithons. BtII occurs as euhedral crystals with straight and well-defined grain boundaries. QzII occurs as millimetre- to centimetre-sized crystals with undulose extinction. S_{3a} is also marked by the SPOs of BtII and SilII; SilII forms elongate crystals (0.2–10 mm) with straight and sharp grain boundaries or elongate, fibrolitic domains.

In metabasites, S_{3a} is marked by Pl + Qz and by AmpI ± GrtII layers. Pl (PlII and PlIII) occurs as subhedral crystals in association with CpxII, locally displaying wavy extinction and deformation twins. AmpI is found as elongated or rhomboid crystals (1–9 mm) that are brown or pale green in colour (Fig. 5e).

Syn-stage 3 leucosomes are defined by the association KfsIII + QzIII +BtIII + GrtIII + RtIII + MnzIII + ZrnIII. Leucosomes display equigranular size distribution with a polygonal shape. BtIII, KfsIII and GrtIII (2–20 mm) have idiomorphic shapes. QzIII has an anhedral shape; the grain size varies from less than 0.5 mm to 1.5 cm. Crystals frequently show undulose extinction, indicating that local deformation occurred after the intrusion. MnzIII and ZrnII occur as millimetre-sized grains with a euhedral shape associated with QzIII, GrtIII and BtIII.

4.b.4. Stage 4

Stage 4 is not perceivable at the scale of the Valpelline unit, and it is generally associated with the static

growth of Chl and Wm in migmatites and by the static replacement of Pl by Ep and Wm in basic granulites. At the valley scale, a millimetre-thick foliation (S$_4$) locally develops; this foliation is marked by Wm and Chl and may be also mylonitic (Pennacchioni & Guermani, 1993; Roda & Zucali, 2008). In the studied area, this structure does not develop, but Chl and Wm statically overgrow the old foliations. The late stage 4 is also characterized by the development of brittle, metre-scale structures as faults and cataclasites.

Chl and Ep may also be found as seals of brittle faults. In these zones, faults and fracture systems produce the disaggregation of the protoliths and the loss of the primary mineralogical and fabric characters.

4.b.4.a. Meso-scale observations

The S$_4$ foliation is marked by greenschist-facies minerals in all rock types. In metapelites, this foliation is expressed by Wm and Chl SPOs; in amphibolite, by green Amp SPO; and in marble, by Chl and Cal SPOs. This deformation phase is not homogeneously distributed within the Valpelline unit because it is localized along metres- to tens-of-metres-thick bands, particularly at the contact between the Arolla and the Valpelline units (Pennacchioni & Guermani, 1993). S$_4$ foliation is parallel to the contact between the Arolla and Valpelline units, and it is subsequently folded by recumbent folds.

4.b.4.b. Micro-scale observations

In metapelites, WmI fine-grained aggregates and irregularly shaped aggregates of EpI partly or completely replace PlI, KfsI, SilI and SilII. ChlI aggregates and fine-grained WmI partly replace all generations of Grt and Bt. Grt porphyroblasts contain WmI- and ChlI-filled fractures (Fig. 5f). ChlI (0.5–3 mm) also forms elongate aggregates in which crystals frequently show wavy extinction. CalI occurs as anhedral grains (0.5–2 mm) with lobate and well-defined grain boundaries.

In metabasites, pale green AmpII partly or completely replaces CpxI, OpxI and AmpI. ChlI aggregates and fine-grained WmI partly replace AmpI and GrtI. WmI fine-grained aggregates and irregularly shaped aggregates of EpI partly or completely replace PlII and PlIII. These newly formed minerals may grow along fractures.

5. Mineral chemistry

Minerals were analysed with an electron microprobe (EMPA: JEOL 8200 Super Probe) and a scanning electron microscope (SEM: Cambridge Stereoscan 360 ISIS 300 Oxford) at the Dipartimento di Scienze della Terra 'A. Desio' – Università degli Studi di Milano. The operating conditions were 20 kV accelerating voltage, a filament intensity of 1.70 A and a probe intensity of 280 pA for EMPA and 15 kV accelerating voltage and a sample current of 190 pA for SEM. Natural silicates were used as standards; matrix corrections were calculated with the ZAF procedure. Representative mineral compositions are reported in the online Supplementary

Material available at http://journals.cambridge.org/geo (Tables S1a–g). Figure 6 shows chemical variations within selected mineral phases with respect to their microdomain occupancy and evolutionary stage. Mineral formulae have been recalculated using JPT (Zucali, 2005), which uses the general recalculation scheme after Deer, Howie & Zussman (1996).

Biotite. Biotite in gneiss and migmatite commonly coexists with ilmenite and shows a linear increase in Ti content from BtI to BtII. Ti content in BtI ranges from 0.342 to 0.798 atoms per formula unit (a.p.f.u.), and it is between 0 and 1 a.p.f.u. in BtII. Among BtII, it is also possible to separate low-Ti minerals from those with high to very high Ti content (Fig. 6). X$_{Mg}$ varies from 0.40 to 0.80 in both BtI and BtII. Al^{VI} content also varies from 0 to 1, and it is closely related with the Ti content variations, as suggested by various studies (Scheurs, 1985; Henry, Guidotti & Thomson, 2005). In metabasite (basic granulite and amphibolite), Bt compositions are generally homogeneous: Ti content varies from 0.52 to 0.72 a.p.f.u., Al^{VI} from 0 to 0.184 a.p.f.u., and X$_{Mg}$ from 0.52 to 0.65.

Amphibole. In metabasites, AmpI (stages 2 and 3) shows a Ca content between 1.5 and 3.5 a.p.f.u., whereas Si varies between 6.71 and 6.71 a.p.f.u. Ti content varies from 1.40 to 3.20 a.p.f.u. In metabasites (stage 3), AmpII displays an Si content between 7 and 8 a.p.f.u., whereas Ti varies between 0 and 1.0 a.p.f.u.

Garnet. GrtI and GrtII in metapelites are Fe-rich (1.68–2.00 a.p.f.u.) with a high Mg content (0.76–1.09 a.p.f.u.) and lower contents of Ca (0.08–0.48 a.p.f.u.) and Mn (0.02–0.06 a.p.f.u.). The Alm content ranges from 59 to 67 %, whereas the Py content varies from 27 to 37 %. GrtII rims commonly show an increase in the Mg and Ca contents compared with GrtI cores.

GrtI (stage 2) in basic granulites and amphibolites shows a Ca content varying from 0.43–0.60 a.p.f.u., a Mg content from 0.58–0.76 a.p.f.u. and an Fe content from 1.70–1.86 a.p.f.u.

Orthopyroxene. OpxI (stage 1 in basic granulite) and OpxII (stage 2 in granulite at the contact with migmatitic gneiss) are hypersthenic, with X$_{Mg}$ increasing from 0.47 (OpxI) to 0.61 (OpxII). Al in Opx ranges from 0.033 to 0.061 a.p.f.u.

Clinopyroxene. CpxI (stage 1 in basic granulites) and CpxII (stage 2 in granulite at the contact with migmatitic gneiss) are clino-hypersthenic, showing X$_{Mg}$ between 0.45 and 0.50. Al in Cpx ranges from 0.048 to 0.061 a.p.f.u.

Feldspars. PlI in metapelite is characterized by a homogeneous Ab content of approximately 0.74. The An content varies in PlI, where it may increase up to 0.32. In metabasite, PlII has a higher An content, which varies from 0.45 to 0.80. Orthoclase occurs in association with PlII (KfsII) and within pegmatite veins (KfsIII).

Spinel. In migmatite (stage 2), spinel is part of a hercynite–spinel–ghanite solid solution, where X$_{Spl}$ varies from 0.25 to 0.39, X$_{Hc}$ from 0.39 to 0.52 and X$_{Gah}$ from 0.15 to 0.36.
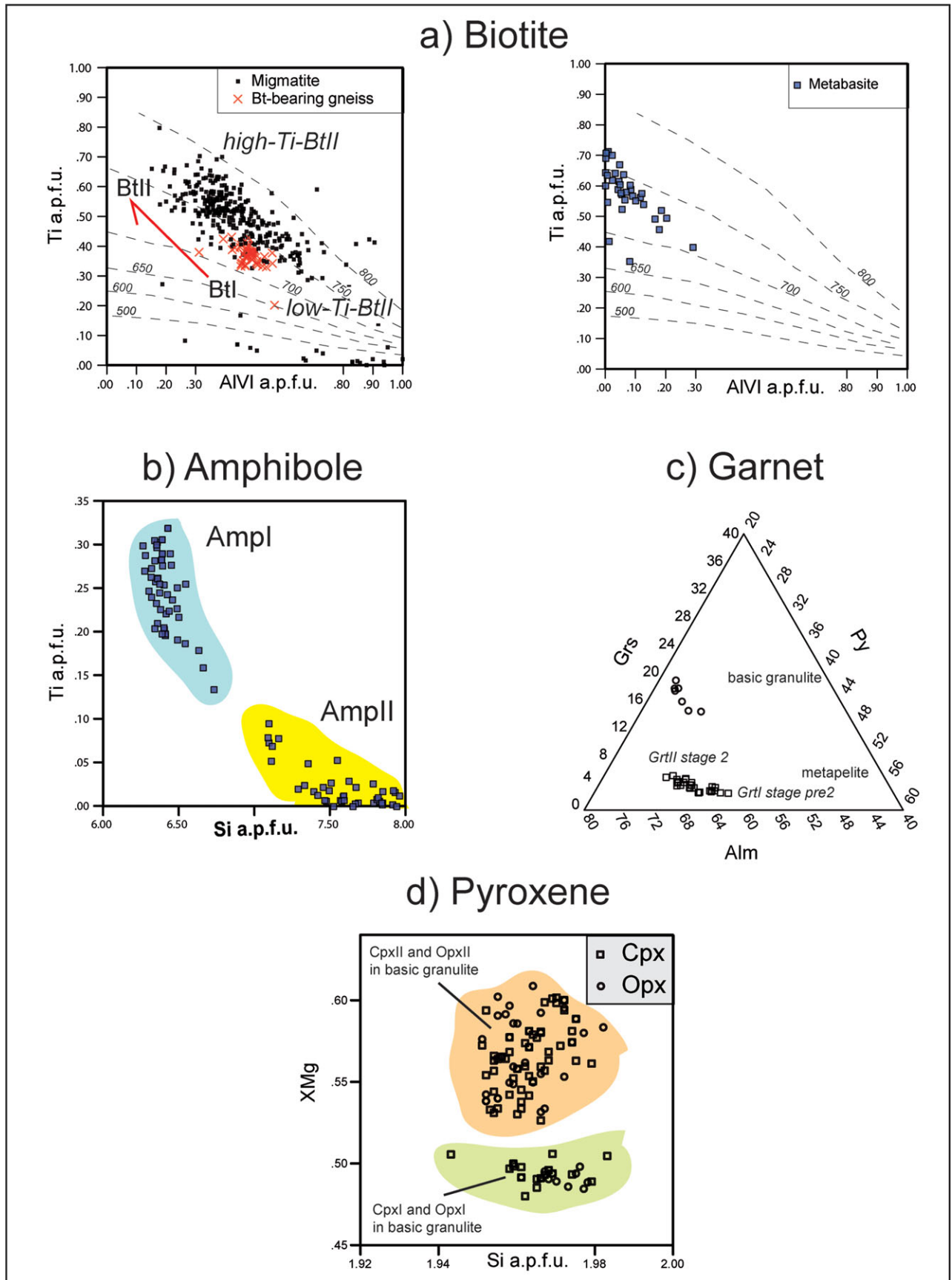
Figure 6. (Colour online) Graphic representation of the chemical composition of selected mineral phases: (a) biotite; $T\,^{\circ}C$ isolines after Henry, Guidotti & Thomson (2005); (b) amphibole; (c) garnet; (d) pyroxene.
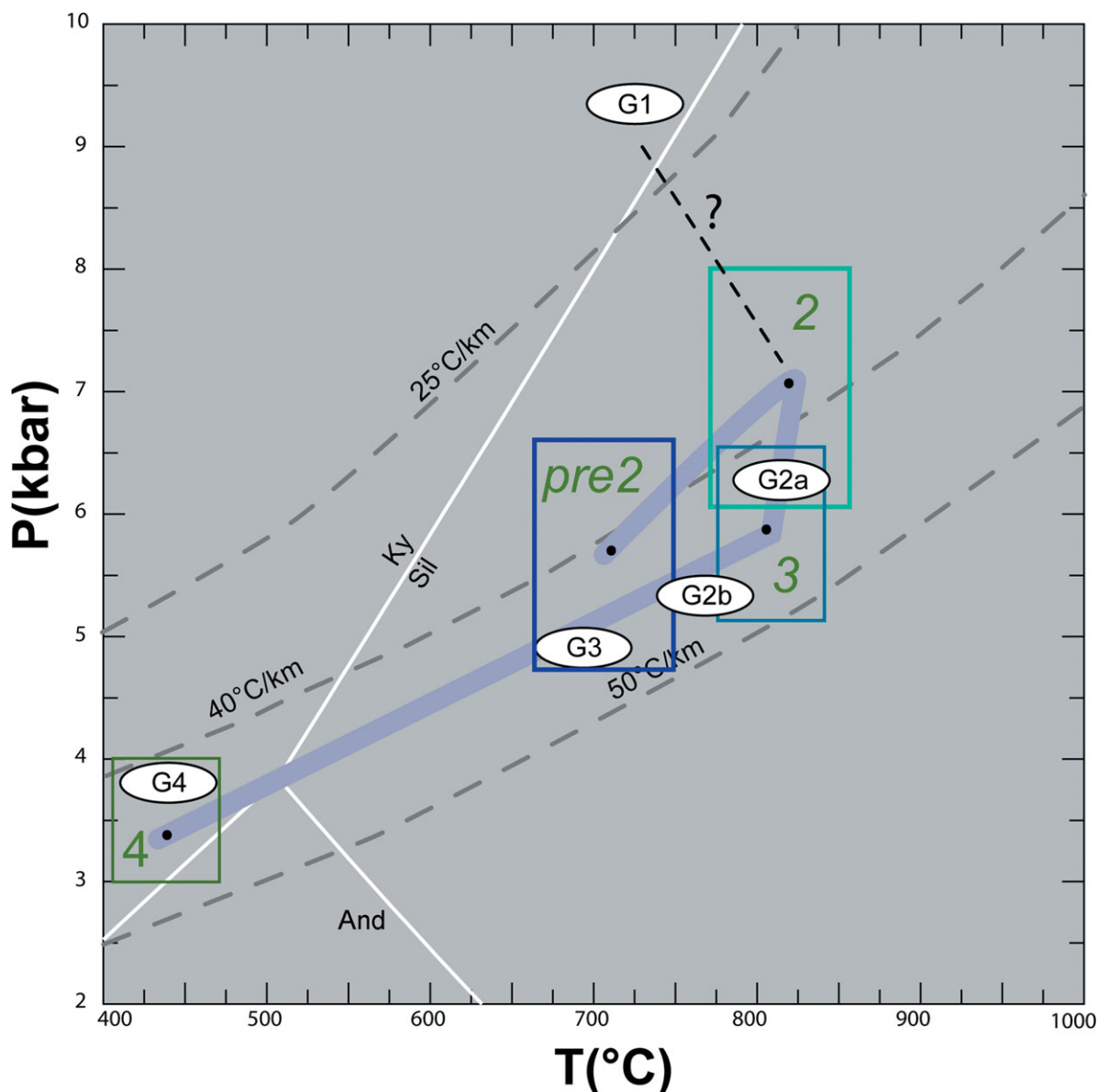
Figure 7. (Colour online) *P–T–t*–d paths reconstructed on the basis of meso- and microstructural relationships and *P–T* estimates. G1, G2a, G2b, G3 and G4 stages from Gardien, Reusser & Marquer (1994); boxes and chronology from this work. 25–40–50 °C km^{-1} geothermal gradients are shown. Ky, And, Sil stability fields calculated using the thermodynamic database of Holland & Powell (1998).

Table S1g in the online Supplementary Material available at http://journals.cambridge.org.geo also reports selected analyses of stage 4 chlorite and white mica. Chl compositions vary in the Mg, Al and Si contents, whereas Wm compositions distinguish two generations that may be discriminated by the variations in the Si, Al, Mg and Fe contents.

6. Estimates of pressure and temperature conditions

Available petrogenetic grids and thermobarometry were used to estimate the physical conditions of metamorphic stages (Fig. 7), as reconstructed by meso- and microstructural analyses. Microstructural analysis allowed for the recognition of reactions that occurred during metamorphic evolution and their relative timing.

Mineral pairs and stable associations were used for thermobarometric estimates (Table 4). Pressure and temperature conditions and the reactions deduced by microstructures are compared with data available from petrogenetic grids. Temperatures were estimated using garnet–biotite Fe–Mg exchange thermometry (Bhattacharya *et al.* 1992; Wu & Cheng, 2006) and using the Ti content in biotite with the calibration of Henry, Guidotti & Thomson (2005). The pressures were estimated using a garnet–aluminosilicate–silica–plagioclase (GASP) barometer for which the calibration of Holdaway (2001) was employed, and a using garnet–plagioclase–biotite–quartz (GPBQ) barometer with the calibration of Hodges & Spear (1982). Average *P–T* estimates were calculated using Thermocalc v. 3.33 (Holland & Powell, 1998) in mode 2; the activities of the end-member minerals from chemical analyses

Table 4. Thermobarometric estimates for the Valpelline rocks, with reference to the method used (see text for calibration references)

stage	sample	T °C ± sd	P kbar (± sd)	rock	method
Pre 2	P55	*741 ± 25*		gneiss	Ti in biotite
	P55		*4.5–6.5*	gneiss	GPBQ
	P55	*658 ± 31*		gneiss	Grt-Bt_HL77
	P55	*710 ± 15*	*4.7*	gneiss	GASP
2	P74_HTi	*819 ± 50*		migmatite	Ti in biotite
	P28–3084	*781 ± 2*		migmatite	Ti in biotite
	P72B-P36	*797 ± 6*		granulite	Ti in biotite
	P74-P55	*873 ± 16*		migmatite+gneiss	Grt-Bt
	P74-P55		*8*	migmatite+gneiss	GASP
	P28	*844 ± 21*		migmatite	Grt-Bt
	P74-P66-P67-P74		*5–8*	migmatite	GPBQ
	P72B-P36	*813 ± 104*	*7.6 ± 1.7*	granulite	avPT
3	P16-P36-P72B-P27-P3083	*855 ± 12*	*5–6.5*	amphibolite	Al-tot Amp
		829 ± 10	*5–6.5*	amphibolite	Pl-Amp
		824 ± 50		amphibolite	Ti-Amp
		780 ± 22		amphibolite	Ti-Bt
4	P55-P3085-P25	*339 ± 16*		migmatite	AlIV-Chl
	P42-P3082-P3083	*455 ± 38*		amphibolite	AlIV-Chl

avPT – Thermocalc v. 3.33 mode 2 calculations using activities from microprobe analysis as input.

were calculated using AX software (Holland, 2000) and used as input.

Stage pre2 is preserved in different lithologies (Bt-bearing gneisses, Opx-bearing granulites, amphibolites and Ol-bearing marbles), and frequently, this stage is associated with the development of the S_{pre2} foliation. Thermobarometric estimates on mineral pairs and stable associations for stage pre2 in Bt-bearing gneiss are shown in Table 4; temperatures are between $703 \pm 42\,°C$, and pressures are in the range of 4.5 to 6.5 kbar. Similar P–T intervals are shown by P–T pseudosections reconstructed for comparable bulk compositions in the model system Na_2O–CaO–K_2O–FeO–MgO–Al_2O_3–SiO_2–H_2O (NCKFMASH) (e.g. White, Powell & Holland, 2001) for the Bt-bearing assemblages in the absence of melt.

During stage 2, a pervasive migmatization affects metapelites, and a centimetre- to millimetre-thick S_2 foliation develops, which is marked by the alternation of leucosome and melanosome. Some microstructures recognized in migmatites (e.g. growth twins and SillII associated with GrtII) suggest crystallization and growth processes from a melt, and these microstructures may be a result of melt-producing continuous reactions involving Bt as a reactant (White, Powell & Holland, 2001; White & Powell, 2002), indicating $T \geq 800\,°C$ and $P > 6$ kbar. The rare appearances of garnet + cordierite + orthopyroxene by biotite-melting reactions have been recently investigated using a P–T pseudosections approach (Johnson, White & Powell, 2008) and in natural rocks (Bhandari *et al*. 2011). Bhandari *et al*. (2011) also observed that garnet grew to the exclusion of cordierite and orthopyroxene in a relatively ferran bulk-rock composition, whereas garnet and cordierite appeared in more magnesian and aluminous compositional domains. The biotite-melting reactions suggested by the authors for the NCKFMASH system are $Bt + Pl + Qz = Grt + Kfs + melt$ (for garnet

alone), $Bt + Sil + Pl + Qz = Grt + Crd + Kfs + melt$ and $Bt + Pl + Qz = Grt + Crd + Kfs + melt$ (for garnet + cordierite), thereby producing mineral associations similar to those that were stable during this stage and indicating $T > 770\,°C$ at $P > 6$ kbar (Johnson, White & Powell, 2008). Gardien, Reusser & Marquer (1994) estimated $P > 5$ kbar at $T > 750\,°C$ for this stage. Thermobarometric estimates on mineral pairs and stable associations of stage 2 in migmatites result in $T = 814 \pm 40\,°C$ and a P interval of 6–8 kbar (Table 4).

Stages 3a and 3b comprise two superimposed deformational phases that rework the pre-existing structures. Both deformational phases are marked by the same metamorphic minerals (BtII + SillII + GrtII layers and QzII + PlII + KfsII lithons). Gardien, Reusser & Marquer (1994) estimated a pressure of 4–6 kbar and temperature of 750–800 °C for these stages, characterized by the assemblage Bt + Sil + Pl + Qz ± Grt ± Kfs in metapelite. On the basis of the absence of cordierite in migmatite and using the experimental curve Phl + Sil + Qz = Mg-Crd (Spear & Cheney, 1989), Gardien, Reusser & Marquer (1994) constrained the lower pressure for the same stages at 5.5 kbar. This curve cross-cuts at 6 kbar the experimental curve between medium pressure and low pressure granulites calibrated by Green & Ringwood (1967). Thermobarometric estimates on mineral pairs and stable associations of stages 3a and 3b in amphibolite indicate temperatures of $822 \pm 31\,°C$ and pressures of 5–6.5 kbar (Table 4). Stage 3 is also characterized by the crystallization of the magmatic assemblage Grt + Bt + Kfs + Qz in leucosomes (i.e. pegmatites). This assemblage is related to the melt-producing reactions involving Bt + Sil + Qz + Pl as reactants at $T > 800\,°C$ and $P > 6$ kbar (White, Powell & Holland, 2001; Johnson, White & Powell, 2008). This P–T estimate agrees with the mesoscopic observations that
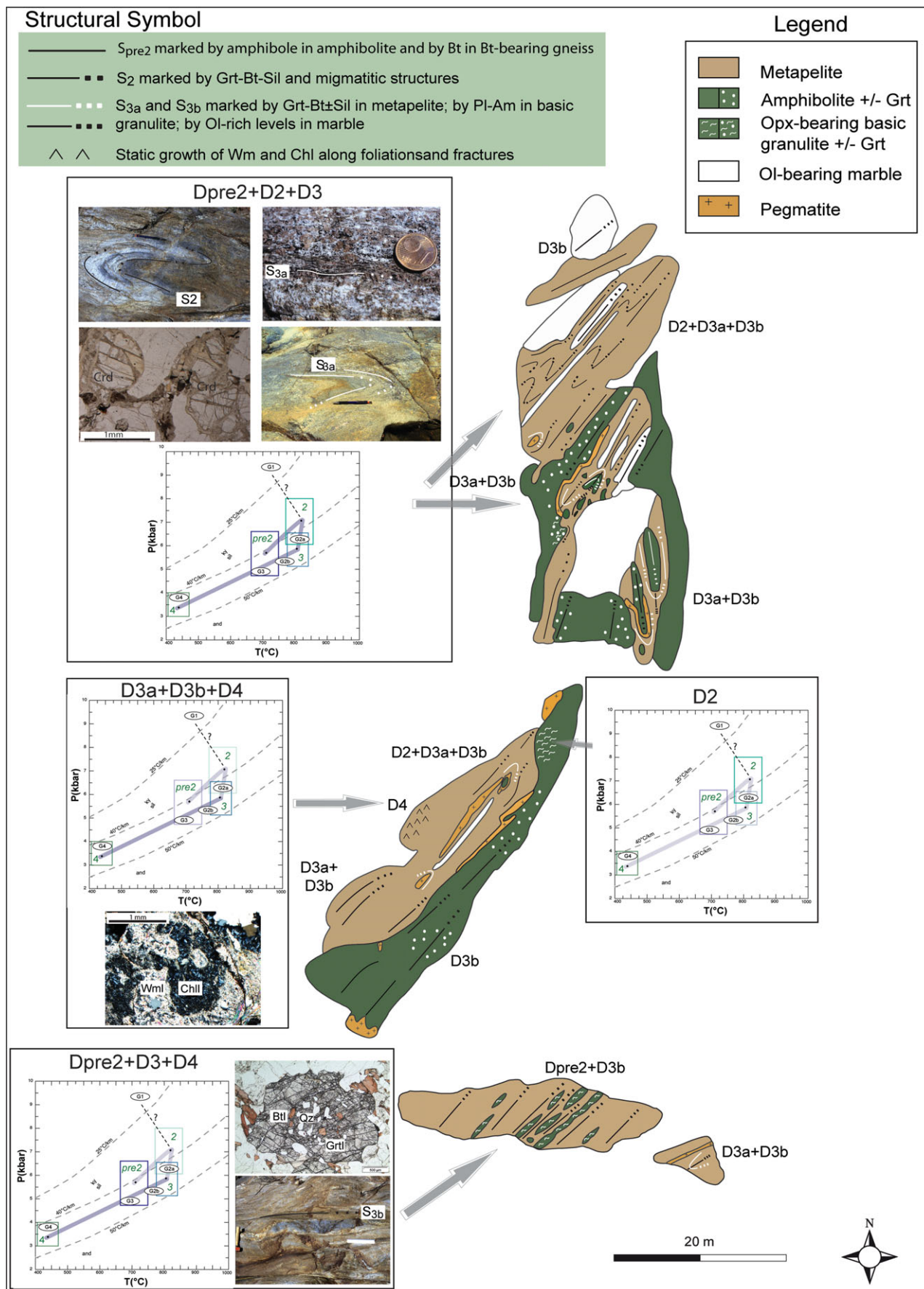
Figure 8. (Colour online) Structural and metamorphic map of the study area, showing metre-scale relationship between lithologies, superimposed structures and relative fabric-supporting minerals related to the recorded metamorphic imprints. On the map, the dots along the foliations trace the relative chronology of superimposed foliations. Mineral assemblages related to successive fabrics in each rock type are represented by differently coloured trajectories and by different symbols associated with the trajectories (Spalla *et al.*

suggest the contemporaneous development of Grt-bearing leucosomes and of the S_2 and S_3 foliations.

During stage 4, WmI and EpI replace Pl, following the reaction $Pl + H_2O = EpI + WmI + Qz$ (Holland & Powell, 1998). Gardien, Reusser & Marquer (1994) described a similar pre-Alpine metamorphic imprint occurring under greenschist facies conditions ($T < 500\,°C$ and $P \approx 3$–4 kbar). $Kfs + Sil + H_2O = Wm + Qz + L$ and $Bt + Kfs + Sil + H_2O = Wm + Qz$ reactions may also indicate the replacement of Sil, Bt and Kfs by WmI and Qz. During the same stage, Bt and Grt are replaced by ChlI, probably through the reaction $Grt + Bt + Sil + H_2O = Chl + Wm + Qz$ (Spear & Cheney, 1989). The AlIV content in the Chl thermometer (Chatelineau, 1988) infers $T = 339 \pm 16\,°C$ in Bt-bearing gneiss and migmatite and $T = 455 \pm 38\,°C$ in amphibolite.

7. Discussion and interpretation

7.a. Tectonometamorphic evolution

The Valpelline unit is characterized by a polyphase evolution from pre-Permian to Alpine age and under granulite to greenschist facies conditions. In the studied area (300×50 m), the deformational and metamorphic imprints are heterogeneously distributed in space, thereby producing a chronological and spatially heterogeneous network of structures and metamorphic associations (Fig. 8). In the studied rocks, the pre-Alpine history is characterized by four evolutionary stages.

Stage pre2 comprises a complex structural and metamorphic evolution prior to stage 2. In this stage, we group several phases of deformation and metamorphism recorded in different lithologies (Ol-bearing marbles, Bt-bearing gneiss, amphibolites, and boudins of Opx-bearing basic granulites within migmatites) and characterized by contrasting P–T conditions. A weak foliation (S_{pre2}) is locally recognizable at the meso- or micro-scale.

Thermobarometric estimates from Bt-bearing gneiss give estimates of $T = 700 \pm 50\,°C$ and $P = 5.7 \pm 1$ kbar (Fig. 7).

In a nearby area of the Valpelline, Gardien, Reusser & Marquer (1994) recognized earlier stages of a high pressure granulite facies evolution in Bt-bearing gneiss, as indicated by kyanite–rutile–alkali feldspar relics in metapelites ($700\,°C$ at 9.3 kbar).

Stage 2 is characterized by the growth of Grt in basic granulites, thereby producing the stable assemblage $Opx + Cpx + Pl + Grt$, whereas in metapelites, migmatitic structures largely develop that are associated with diffuse melt-producing reactions. The temperature ($810 \pm 40\,°C$) and pressure (7 ± 1

kbar) attained during stage 2 (Fig. 7) indicates a > 35–$40\,°C$ km^{-1} geothermal gradient.

Stages 3a and 3b correspond to a progressive deformation (S_{3a} and S_{3b} foliations and isoclinal folds) under amphibolite to granulite metamorphic conditions that is well preserved in metabasites and metapelites, where these stages are associated with the production of Grt-bearing melts (metre-thick leucosome bodies and veins). The temperature ($800 \pm 30\,°C$) and pressure (6 ± 0.7 kbar) attained during stage 3 (Fig. 7) still indicates a high geothermal gradient $> 40\,°C$ km^{-1}.

The last recorded stage of the evolution is stage 4. Stage 4 is not pervasive, and it is associated with the static growth of Chl and Wm on Bt. This stage occurs under greenschist facies conditions ($T = 430 \pm 30\,°C$ at $P = 3.5 \pm 0.5$ kbar). During this stage, faults and cataclasites also affect all lithologies, as shown for the surrounding rocks of the Arolla unit (Roda & Zucali, 2008).

7.b. Age constraints and geodynamic implications

Several considerations may be proposed for the pre-Alpine evolution described above.

Stage pre2 reflects a Variscan high thermal gradient, as inferred from abundant basic granulites and Bt-bearing gneiss. Gardien, Reusser & Marquer (1994) recognized earlier stages of a high pressure granulite facies evolution that may have recorded the crustal thickening associated with the Variscan collision thickening. The earlier stages (Gardien, Reusser & Marquer, 1994) and those found in the present study may indicate that separate tectonic subunits were decoupled during the Variscan. The later juxtaposition of these stages would imply either a collisional extrusion of the lower subunit at the end of the Variscan or a Permian extension during lithospheric thinning and continental rifting. Further studies (i.e. a geochronological study of the kyanite-bearing metapelites found by Gardien, Reusser & Marquer, 1994) are needed to encompass this stage and might help to distinguish between the two hypotheses proposed.

Stages 2 and 3 are characterized by melt-producing reactions and migmatites and by the emplacement of a large amount of melt along veins and dykes. This evolution and the related thermal gradient may be ascribed to the late-Variscan–Permian high thermal event, which is widely reported in the Variscan history of the European continental crust and generally associated with the post-collisional thinning to Permo-Triassic rifting (Weber, 1984; Lardeaux & Spalla, 1991; Schuster & Stüwe, 1991; Bonin *et al.* 1993; Müntener & Hermann, 2001). Generally, the intrusion of large igneous bodies across the pre-Alpine continental crust is also associated with this evolution (Bonin *et al.* 1993;

2000). Also shown are heterogeneous P–T–t–d memories, registered in adjacent rock domains. The figure shows distribution of domains where structural and metamorphic imprints are better recorded with respect to degree of fabric development. Pencil for scale is 13 cm long; coin is 1 cm in diameter; ruler is 20 cm long; and hammer is 40 cm long.

Marotta & Spalla, 2007; Marotta, Spalla & Gosso, 2009 and references therein). In the case of the Valpelline unit, Permian intrusions occur within the adjacent Arolla unit, which is composed of granitic to gabbroic igneous intrusions of Permian age (i.e. *Collon* and *Cervino gabbros*: 250 ± 5 Ma, K–Ar, Rb–Sr (Dal Piaz, De Vecchi & Hunziker, 1977); 284 ± 0.6 Ma, U–Pb (Monjoie *et al.* 2005); *Arolla granites*: 289 Ma (Bussy *et al.* 1998)). Within the Arolla intrusives, several roof pendants and xenolite fragments of various sizes (a few to hundreds of metres in length) were found. These intrusives are also represented by amphibolites, biotite- and garnet-bearing gneisses and acid granulites (Diehl, Masson & Stutz, 1952; Roda & Zucali, 2008). The lithological similarities between the Arolla xenolites and Valpelline lithotypes (acid granulites, gneisses and amphibolites) along with the high temperature imprint recorded in the described lithotypes suggest that the Valpelline unit is older than the Permian Arolla intrusions (i.e. 250–290 Ma).

Permian magmatism and HT–LP metamorphism affecting the Alpine continental crust have been related to the late orogenic collapse of the Variscan belt (Malavielle *et al.* 1990; Ledru *et al.* 2001) or as a consequence of lithospheric thinning leading to continental rifting, as proposed for the Austroalpine and Southalpine domains (Diehl, Masson & Stutz, 1952; Lardeaux & Spalla, 1991; Diella, Spalla & Tunesi, 1992; Müntener & Hermann, 2001; Schuster & Stüwe, 2008).

The second hypothesis appears more suitable because at the Carboniferous/Permian boundary, the Palaeozoic plate convergence is replaced by a transensional to extensional tectonic regime, which promoted the break-up of Pangaea (Marotta & Spalla, 2007; Schuster & Stüwe, 2008). In the Austroalpine and Southalpine domains, the Permian radiometric ages have been interpreted as representing metamorphic and igneous markers of earlier stages of Mesozoic rifting (Lardeaux & Spalla, 1991; Quick *et al.* 1992; Dal Piaz, 1993; Thoni & Miller, 2000), whereas the Triassic ages have been interpreted as either minimal ages of thermal pulses during extension-related decompression (Vavra, Schmid & Gebauer, 1999) or resulting from a later regional thermal event (Lu *et al.* 1997). In the Southalpine domain the stratigraphic sequences also document late Carboniferous to Carnian transtension followed by Carnian to Cretaceous rifting to drifting (Gaetani *et al.* 1998; Muttoni *et al.* 2003).

The high thermal gradient and the extensive production and segregation of melt recorded in the metapelites of the Valpelline unit seem to support the high thermal regime associated with the syn-rifting crustal thinning. Dating of accessory phases (allanite, zircon and titanite) in metasediments amalgamated with the gneisses of the Arolla Series, points to Permian metamorphism between ∼ 300 and 265 Ma (Manzotti *et al.* 2012). Absolute age data for the Valpelline unit are too sparse and difficult to interpret (Hunziker,

1974) for a confident constraining of the tectonic evolution. The only age constraints are generally inferred from lithological similarities and structural relationships with adjacent units (e.g. Arolla) or on the basis of lithological–metamorphic comparisons with other units of the Alpine–European chain, which are characterized by similar lithostratigraphic, structural or metamorphic imprints (Spalla & Marotta, 2007; Schuster & Stüwe, 2008; Marotta, Spalla & Gosso, 2009). Preliminary U–Pb dating on zircon from a pegmatite in the Valpelline unit indicates the Permian period (∼ 270 Ma) for the high temperature metamorphism (Zucali *et al.* 2011). Reliable age data would be crucial to relate the local thermal and mechanical history to the geodynamics at the lithosphere scale during Variscan to Permian times.

The well-preserved structural and metamorphic history of this small portion of the Valpelline basement makes possible a first attempt at an interpretation of the pre-Alpine geodynamics of this unit. An extension of this approach to adjacent portions of the Valpelline unit will help to shed light on the transition between the late orogenic collapse of the Variscan chain and the lithospheric thinning that promoted the opening of the Tethys Ocean.

References

ARGAND, E. 1906. Sur la carte tectonique du Massif de la Dent Blanche. *Comptes Rendus de l'Académie des Sciences Paris* **142**, 527–29.

BALLÈVRE, M. & KIENAST, J. R. 1987. Decouverte et signification de parageneses a grenat-amphibole bleu dans la couverture mesozoique de la nappe de la Dent-Blanche (Alpes Occidentales). *Comptes Rendus de l'Académie des Sciences Paris* **305**, 43–6.

BHANDARI, A., PANT, N. C., BHOWMIK, S. K. & GOSWAMI, S. 2011. ∼1.6 Ga ultrahigh-temperature granulite metamorphism in the Central Indian Tectonic Zone: insights from metamorphic reaction history, geothermobarometry and monazite chemical ages. *Geological Journal* **46**, 198–216.

BHATTACHARYA, A., MOHANTY, L., MAJI, A., SEN, S. K. & RAITH, M. 1992. Non-ideal mixing in the phlogopite-annite binary: constraints from experimental data on Mg-Fe partitioning and a reformulation of the biotite-garnet geothermometer. *Contributions to Mineralogy and Petrology* **111**, 87–93.

BOHLEN, S. R. 1987. Pressure-temperature-time paths and a tectonic model for the evolution of granulites. *Journal of Geology* **95**, 617–32.

BONIN, B., BRAENDLEIN, P., BUSSY, F., DESMONS, J. & EGGENBERGER, U. 1993. Late Variscan magmatic evolution of the Alpine basement. In *Pre-Mesozoic Geology in the Alps* (eds J. F. von Raumer & F. Neubauer), pp. 171–201. Berlin & Heidlberg: Springer-Verlag.

BUSSY, F., VENTURINI, G., HUNZIKER, J. C. & MARTINOTTI, G. 1998. U-Pb ages of magmatic rocks of the Western Austroalpine Dent-Blanche-Sesia Unit. *Schweizerische Mineralogische und Petrographische Mitteilungen* **78**, 163–68.

CABY, R., KIENAST, J. R. & SALIOT, P. 1978. Structure, metamorphism and model of tectonic evolution of the Western Alps. *Revue de Geographie Physique et de Geologie Dynamique* **20**, 307–22.

CANEPA, A., CASTELLETTO, M., CESARE, B., MARTIN, S. & ZAGGIA, L. 1990. The Austroalpine Mont Mary nappe (Italian Western Alps). *Memorie di Scienze Geologiche* **42**, 1–17.

CHATELINEAU, M. 1988. Cation site occupancy in chlorites and illites as a function of temperature. *Clay Minerals* **23**, 471–85.

DAL PIAZ, G. V. 1993. Evolution of Austrolapine and Upper Penninic basement in the northwestern Alps from Variscan convergence to post-Variscan extension. In *Pre-Mesozoic Geology in the Alps* (eds J. F. von Raumer & F. Neubauer), pp. 325–42. Berlin & Heidlberg: Spring-Verlag.

DAL PIAZ, G. V., DE VECCHI, G. & HUNZIKER, J. C. 1977. The Austroalpine layered gabbros of the Matterhorn and Mt. Collon-Dents de Bertol. *Schweizerische Mineralogische und Petrographische Mitteilungen* **57**, 59–88.

DEER, W. A., HOWIE, R. A. & ZUSSMAN, J. 1996. *An Introduction to the Rock-Forming Minerals*. New York: Prentice Hall.

DE LEO, S., BIINO, G. & COMPAGNONI, R. 1987. Riequilibrazioni metamorfiche alpine nella serie di Valpelline e di Arolla a Nord di Bionaz (Valpelline-Aosta). *Rendiconti della Società Italiana di Mineralogia e Petrologia* **42**, 181–82.

DE GIUSTI, F., DAL PIAZ, G. V., MASSIRONI, M. & SCHIAVO, A. 2003. Carta geotettonica della Valle d'Aosta. *Memorie di Scienze Geologiche* **55** (2003/2004), 129–49.

DIEHL, E. A., MASSON, R. & STUTZ, A. H. 1952. Contributo alla conoscenza del ricoprimento della Dent Blanche. *Memorie degli Istituti di Geologia e Mineralogia dell'Università di Padova* **17**, 1–52.

DIELLA, V., SPALLA, M. I. & TUNESI, A. 1992. Contrasting thermomechanical evolutions in the southalpine metamorphic basement of the Orobic Alps (Central Alps, Italy). *Journal of Metamorphic Geology* **10**, 203–19.

ELLIS, D. J. 1987. Origin and evolution of granulites in normal thickened crusts. *Geology* **15**, 167–70.

GAETANI, M., GNACOLLINI, M., JADOUL, F. & GARZANTI, E. 1998. Multiorder sequence stratigraphy in the Triassic system of the western Southern Alps. In *Mesozoic and Cenozoic Sequence Stratigraphy of European Basins* (eds P. C. De Graciansky, J. Hardenbol, T. Jacquin & P. R. Vail), pp. 701–17. Society for Sedimentary Geology (SEPM) Special Publication 60.

GALLI, A., LE BAYON, B., SCHMIDT, M. W., BURG, J. P., REUSSER, E., SERGEEV, S. A. & LARIONOV, A. 2012. U-Pb zircon dating of the Gruf Complex: disclosing the late Variscan granulitic lower crust of Europe stranded in the Central Alps. *Contributions to Mineralogy and Petrology* **163**, 353–78.

GARDIEN, V. 1994. Occurrence of kyanite in the gneisses from the Valpelline Series (Dent-Blanche Nappe, Western Alps). *Comptes Rendus de l'Academie des Sciences Paris, Serie 2* **319**, 899–905.

GARDIEN, V., REUSSER, E. & MARQUER, D. 1994. Pre-Alpine metamorphic evolution of the gneisses from the Valpelline Series (Western Alps, Italy). *Schweizerische Mineralogische und Petrographische Mitteilungen* **74**, 489–502.

GREEN, D. H. & RINGWOOD, A. E. 1967. An experimental investigation of the gabbro to eclogite transformation and its petrological applications. *Geochimica et Cosmochimica Acta* **31**, 767–833.

HARLEY, S. L. 2008. Refining the P-T records of UHT crustal metamorphism. *Journal of Metamorphic Geology* **26**, 125–54.

HENRY, B., GUIDOTTI, C. V. & THOMSON, J. A. 2005. The Ti-saturation surface for low-to-medium pressure metapelitic biotite: implications for geothermometry and Ti-substitution mechanisms. *American Mineralogist* **90**, 316–28.

HODGES, K. V. & SPEAR, F. S. 1982. Geothermometry, geobarometry and the Al_2SiO_5 triple point at Mt Moosilauke, New Hampshire. *American Mineralogist* **67**, 1118–34.

HOLDAWAY, M. J. 2001. Recalibration of the GASP geobarometer in light of recent garnet and plagioclase activity models and versions of the garnet-biotite geothermometer. *American Mineralogist* **86**, 1117–29.

HOLLAND, T. 2000. AX: a program to calculate activities of mineral end members from chemical analyses which uses the activity models outlined in Holland & Powell (1998). http://www.esc.cam.ac.uk/research/research-groups/holland/ax

HOLLAND, J. B. & POWELL, R. 1998. An internally consistent thermodynamic data set for phases of petrologic interest. *Journal of Metamorphic Geology* **16**, 309–43.

HUNZIKER, J. C. 1974. Rb-Sr and K-Ar determination and the Alpine tectonic history of the Western Alps. *Memorie degli Istituti di Geologia e Mineralogia dell'Università di Padova* **31**, 1–54.

JOHNSON, T. E., WHITE, R. W. & POWELL, R. 2008. Partial melting of metagreywacke: a calculated mineral equilibria study. *Journal of Metamorphic Geology* **26**, 837–53.

KIENAST, J. R. & NICOT, E. 1971. Presence of a disthene paragenesis and chloritoid probably Alpine in sillimanite gneiss, garnet and cordierite of Valpelline (Val Daoste, Italy). *Comptes Rendus Hebdomadaires des Seances de l'Academie des Sciences Serie D* **272**, 1836–40.

KRIEGSMAN, L. M. & ALVAREZ-VALERO, A. M. 2010. Melt-producing versus melt-consuming reactions in pelitic xenoliths and migmatites. *Lithos* **116**, 310–20.

LARDEAUX, J. M. & SPALLA, M. I. 1991. From granulites to eclogites in the Sesia Zone (Italian Western Alps) – a record of the opening and closure of the Piedmont Ocean. *Journal of Metamorphic Geology* **9**, 35–59.

LEDRU, P., COURRIOUX, G., DALLAIN, C., LARDEAUX, J. M., MONTEL, J. M., VANDERHAEGHE, O. & VITEL, G. 2001. The Velay dome (French Massif Central): melt generation and granite emplacement during orogenic evolution. *Tectonophysics* **342**, 207–37.

LU, M. H., HOFMANN, A. W., MAZZUCCHELLI, M. & RIVALENTI, G. 1997. The mafic-ultramafic complex near Finero (Ivrea-Verbano Zone). 2. Geochronology and isotope geochemistry. *Chemical Geology* **140**, 223–35.

MALAVIELLE, J., GUIHOT, P., COSTA, S., LARDEAUX, J. M. & GARDIEN, V. 1990. Collapse of the thickened Variscan crust in the French Massif Central: Mont Pilat extensional shear zone and St. Etienne Late Carboniferous basin. *Tectonophysics* **177**, 139–49.

MALUSÀ, M., FACCENNA, C., GARZANTI, E. & POLINO, R. 2011. Divergence in subduction zones and exhumation

of high pressure rocks (Eocene Western Alps). *Earth and Planetary Science Letters* **310**, 21–32.

MANZOTTI, P. 2011. Petro-structural map of the Dent Blanche tectonic system between Valpelline and Valtournenche valleys, Western Italian Alps. *Journal of Maps* **v2011**, 340–52.

MANZOTTI, P., RUBATTO, D., DARLING, J., ZUCALI, M., CENKI-TOK, B. & ENGI, M. 2012. From Permo-Triassic lithospheric thinning to Jurassic rifting at the Adriatic margin: petrological and geochronological record in Valtournenche (Western Italian Alps). *Lithos* **146–147**, 276–92.

MARSCHALL, H. R., KALT, A. & HANEL, M. 2003. P-T evolution of a Variscan lower-crustal segment: a study of granulites from the Schwarzwald, Germany. *Journal of Petrology* **44**, 227–53.

MAROTTA, A. M. & SPALLA, M. I. 2007. Permian-Triassic high thermal regime in the Alps: result of late Variscan collapse or continental rifting? Validation by numerical modeling. *Tectonics* **26**, TC4016, doi: 10.1029/2006TC002047, 27 pp.

MAROTTA, A. M., SPALLA, M. I. & GOSSO, G. 2009. Upper and lower crustal evolution during lithospheric extension: numerical modelling and natural footprints from the European Alps. *Extending a Continent: Architecture, Rheology and Heat Budget* (eds U. Ring & B. Wernicke), pp. 33–72. Geological Society of London, Special Publication no. 321.

MONJOIE, P., BUSSY, F., LAPIERRE, H. & PFEIFER, H. R. 2005. Modeling of in-situ crystallization processes in the Permian mafic layered intrusion of Mont Collon (Dent Blanche nappe, western Alps). *Lithos* **83**, 317–46.

MÜNTENER, O. & HERMANN, J. 2001. The role of lower crust and continental upper mantle during formation of non-volcanic passive margins: evidence from the Alps. In *Non-Volcanic Rifting of Continental Margins: A Comparison of Evidence from Land and Sea* (eds. R. C. L. Wilson, R. B. Whitmarsh, B. Taylor & N. Froitzheim), pp. 267–88. Geological Society of London, Special Publication no. 187.

MUTTONI, G., KENT, D. V., GARZANTI, E., BRACK, P., ABRAHAMSEN, N. & GAETANI, M. 2003. Early Permian Pangea 'B' to Late Permian Pangea 'A'. *Earth and Planetary Science Letters* **215**, 379–94.

PASSCHIER, C. W. & TROUW, R. A. J. 2005. *Microtectonics*. Berlin: Springer, 366 pp.

PENNACCHIONI, G. & GUERMANI, A. 1993. The mylonites of the Austroalpine Dent Blanche nappe along the northwestern side of the Valpelline Valley (Italian Western Alps). *Memorie di Scienze Geologiche* **45**, 37–55.

PIN, C. & VIELZEUF, D. 1983. Granulites and related rocks in Variscan median Europe: a dualistic interpretation. *Tectonophysics* **93**, 47–74.

PIN, C. & VIELZEUF, D. 1988. Les granulites de haute-pression d'Europe moyenne témoins d'une subduction éo-hercynienne. Implications sur l'origine des goupes leptyno-amphibolitiques. *Bulletin de la Societe Geologique de France* **1**, 3–20.

QUICK, J. E., SINIGOI, S., NEGRINI, L., DEMARCHI, G. & MAYER, A. 1992. Synmagmatic deformation in the underplated igneous complex of the Ivrea-Verbano Zone. *Geology* **20**, 613–16.

RODA, M. & ZUCALI, M. 2008. Meso and microstructural evolution of the Mont Morion metaintrusives complex (Dent Blanche nappe, Austroalpine domain, Valpelline, Western Italian Alps). *Italian Journal of Geosciences* **127**, 105–23.

RODA, M. & ZUCALI, M. 2011. Tectono-metamorphic map of the Mont Morion Permian metaintrusives (Mont Morion – Mont Collon – Matterhorn Complex, Dent Blanche Unit), Valpelline – Western Italian Alps. *Journal of Maps* **v2011**, 519–35.

SAWYER, E. W. 2008. *Working with Migmatites*. Short Course Series: Mineralogical Association of Canada, vol. 38. Quebec: Mineralogical Association of Canada, 158 pp.

SCHEURS, J. 1985. Prograde metamorphism of metapelites, garnet-biotite thermometry and prograde change of biotite chemistry in high grade rocks of West Uusimaa, southwest Finland. *Lithos* **18**, 69–80.

SCHUSTER, R. & STÜWE, K. 2008. Permian metamorphic event in the Alps. *Geology* **36**, 603–6.

SEARLE, M. P., COTTLE, J. M., STREULE, M. J. & WATERS, D. J. 2010. Crustal melt granites and migmatites along the Himalaya: melt source, segregation, transport and granite emplacement mechanisms. *Earth and Environmental Science Transactions of the Royal Society of Edinburgh* **100**, 219–33.

SPALLA, M. I., GOSSO, G., MAROTTA, A. M., ZUCALI, M. & SALVI, F. 2010. Analysis of natural tectonic systems coupled with numerical modelling of the polycyclic continental lithosphere of the Alps. *International Geology Review* **52**, 1268–302.

SPALLA, M. I. & MAROTTA, A. M. 2007. P-T evolutions vs. numerical modelling: a key to unravel the Paleozoic to early-Mesozoic tectonic evolution of the Alpine area. *Periodico di Mineralogia* **76**, 267–308.

SPALLA, M. I., SILETTO, G. B., DI PAOLA, S. & GOSSO, G. 2000. The role of structural and metamorphic memory in the distinction of tectono-metamorphic units: the basement of the Como lake in the Southern Alps. *Journal of Geodynamics* **30**, 191–204.

SPALLA, M. I., ZUCALI, M., DI PAOLA, S. & GOSSO, G. 2005. A critical assessment of the tectono-thermal memory of rocks and definition of tectono-metamorphic units: evidence from fabric and degree of metamorphic transformations. In *Deformation Mechanisms, Rheology and Tectonics: From Minerals to the Lithosphere* (eds D. Gapais, J. P. Brun & P. R. Cobbold), pp. 227–47. Geological Society of London, Special Publication no. 243.

SPEAR, F. S. & CHENEY, J. T. 1989. A petrogenetic grid for pelitic schists in the system SiO_2-Al_2O_3-FeO-MgO-K_2O-H_2O. *Contributions to Mineralogy and Petrology* **101**, 149–64.

THONI, M. & MILLER, C. 2000. Permo-Triassic pegmatites in the eo-Alpine eclogite-facies Koralpe complex, Austria: age and magma source constraints from mineral chemical, Rb-Sr and Sm-Nd isotope data. *Schweizerische Mineralogische und Petrographische Mitteilungen* **80**, 169–86.

TURNER, F. J. & WEISS, L. E. (eds). 1963. *Structural Analysis of Metamorphic Tectonites*. New York: MacGraw-Hill.

VAVRA, G., SCHMID, R. & GEBAUER, D. 1999. Internal morphology, habit and U-Th-Pb microanalysis of amphibolite-to-granulite facies zircons: geochronology of the Ivrea Zone (Southern Alps). *Contributions to Mineralogy and Petrology* **134**, 380–404.

VERNON, H. V. (ed.) 2004. *A Practical Guide to Rock Microstructure*. Cambridge: Cambridge University Press.

VERNON, R. & CLARKE, G. 2008. *Principles of Metamorphic Petrology*. Cambridge: Cambridge University Press.

VON RAUMER, J. F., STAMPFLI, G. A. & BUSSY, F. 2003. Gondwana-derived microcontinents – the constituents

of the Variscan and Alpine collisional orogens. *Tectonophysics* **365**, 7–22.

WEBER, K. 1984. Variscan events: early Palaeozoic continental rift metamorphism and late Palaeozoic crustal shortening. In *Variscan Tectonics of the North Atlantic Region* (eds d. H. W. Hutton & D. J. Sanderson), pp. 3–23. Geological Society of London, Special Publication no. 14.

WHITE, R. W. & POWELL, R. 2002. Melt loss and the preservation of granulite facies mineral assemblages. *Journal of Metamorphic Geology* **20**, 621–32.

WHITE, R. W., POWELL, R. & HOLLAND, J. B. 2001. Calculation of partial melting equilibria in the system Na_2O-CaO-K_2O-FeO-MgO-Al_2O_3-SiO_2 (NCKFMASH). *Journal of Metamorphic Geology* **19**, 139–53.

WHITNEY, D. L. & EVANS, B. W. 2010. Abbreviation for names of rock-forming minerals. *American Mineralogist* **95**, 185–87.

WU, C. & CHENG, B. 2006. Valid garnet-biotite (GB) geothermometry and garnet-aluminum silicate-plagioclase-quartz (GASP) geobarometry in metapelitic rocks. *Lithos* **89**, 1–23.

ZUCALI, M. 2005. JPT-Mineral formula calculation and geothermobarometry. http://users.unimi.it/mzucali/dev/java/JPT.htm

ZUCALI, M. 2011. Coronitic microstructures in patchy eclogitised continental crust: the Lago della Vecchia pre-Alpine metagranite (Sesia-Lanzo Zone, Western Italian Alps). In *The Science of Microstructure – Part II* (eds M. A. Forster & J. D. Fitz Gerald). *Journal of the Virtual Explorer* **38**, paper 5.

ZUCALI, M., MANZOTTI, P., DIELLA, V., PESENTI, C., RISPLENDENTE, A., DARLING, J. & ENGI, M. 2011. Permian tectonometamorphic evolution of the Dent Blanche Unit (Austroalpine domain, Western Italian Alps). *Rendiconti Online Società Geologica Italiana* **15**, 133–36.